Sustainable Materials and Technologies 40 (2024) e00826

Contents lists available at ScienceDirect

Sustainable Materials and Technologies

journal homepage: www.elsevier.com/locate/susmat

An extensive catalytic potential of sustainable TiO_2-based materials fabricated via flame spray pyrolysis: A comprehensive review

Mohammed Ismael [a,*], Anuradha Sharma [b], Naveen Kumar [b]

[a] Electrical Energy Storage System, Gottfried Wilhelm Leibniz Universität Hannover, Welfengarten 1, 30167 Hannover, Germany
[b] Department of Chemistry, Maharshi Dayanand University, Rohtak 124001, India

ARTICLE INFO

Keywords:
TiO_2 catalyst
Photocatalysis
Flame spray pyrolysis
Thermocatalysis
Electrocatalysis
Organic transformation

ABSTRACT

TiO_2-based materials have been extensively studied and explored in the field of catalysis. However, pristine TiO_2 exhibits a wide energy band gap and fast charge recombination, restricting their large-scale applications. Their performance can be influenced by synthesis methods, doping, and by making composite. Among them, modifying the synthesis techniques, as well as the variables and settings that result in the preparation of highly active materials, is the most crucial stage in having these materials with superior catalytic activity. In contrast to the conventional synthesis approaches, flame spray pyrolysis (FSP), is found particularly simple, efficient, highly scalable, and appropriate for online continuous production and can be considered a promising approach for the fabrication of TiO_2-based nanomaterials having controllable morphologies and composition. This review summarizes for the first time the recent advancements in TiO_2-based materials synthesized via the FSP and their wide-ranging potential catalytic applications including photocatalysis, thermocatalysis, catalysis, and organic transformation. After a brief introduction to the conventional synthesis methods, the fundamentals of the FSP method, equipment, and components were highlighted. Finally, we critically analyze the potential advantages and challenges associated with flame spray pyrolysis, considered as a synthesis method for nanostructured materials. We carefully consider the prospects and limitations of FSP and emphasize key areas for future research and advanced developments in this field.

1. Introduction

The question of how to obtain enough sustainable environment and clean energy solutions has become a topic of utmost importance on a global scale due to the expansion of the world's population and the relentless development of contemporary industry [1,2]. Thus, environmental pollution, fossil fuel depletion, and high energy consumption have recently emerged as three of the biggest global issues [3,4]. Additionally, as fossil fuels like coal, petroleum, and natural gases are consumed more frequently, a significant amount of CO_2 is released into the atmosphere, contributing significantly to global warming, and raising the temperature of the planet [5,6]. Therefore, the need for energy forces us to look for renewable and eco-friendly alternatives to augment and eventually diminish our reliance on fossil fuels. Solar energy is considered one of the most promising ways to lessen the strain on the environment and the energy supply since it is affordable, abundant, and renewable. As a result, it is very desirable to utilize photocatalytic processes to gather solar energy and convert it into usable energy [7,8]. Currently, it is widely acknowledged that hydrogen may be the most viable and optimal option for addressing the triple problems of atmospheric pollution, exhaustion, and the effects of global warming and climate change [9]. The two most popular processes for producing hydrogen from fossil fuels are pyrolysis and hydrocarbon reforming. These methods, which supply almost all the hydrogen needs, are the most sophisticated and popular ones. As of right now, approximately 48% of hydrogen production comes from natural gas, while 30% is derived from heavy oils and naphtha. Additionally, around 18% of hydrogen is generated from coal [10–12] (Fig. 1) [13]. The fossil fuel technique has a significant environmental impact and can result in serious air pollution owing to CO_2 emissions, as opposed to the renewable hydrogen generation pathways (Fig. 1). Thus, the researchers are motivated to create new and modern procedures and look for new energy sources not only because of environmental concerns but also because of the rise in energy consumption.

Among these developed methods, hydrogen production by photocatalytic water splitting may be regarded as a renewable and clean

* Corresponding author.
E-mail address: ismael@ifes.uni-hannover.de (M. Ismael).

https://doi.org/10.1016/j.susmat.2024.e00826
Received 29 September 2023; Received in revised form 1 December 2023; Accepted 9 January 2024
Available online 10 January 2024
2214-9937/© 2024 The Authors. Published by Elsevier B.V. This is an open access article under the CC BY-NC license (http://creativecommons.org/licenses/by-nc/4.0/).

source of energy as it can be achieved by using water and solar light irradiation [14]. Moreover, recent studies have shown that photocatalytic solar H_2 production emits almost little air pollution and global warming [15], and it is simple to store [16]. Therefore, H_2 is viewed as a potentially significant source of energy in the future because it is nontoxic and capable of producing high levels of energy from renewable natural resources like water and solar energy, both of which are clean and durable sources of energy [17]. Since the pioneering research done by the Japanese researchers Fujishima and Honda (1972) concerning the photoelectrochemical water splitting utilizing TiO_2 and Pt electrodes in the presence of UV light illumination, then, various semiconductor materials including oxides such as SnO_2 [18], ZrO_2 [19], TiO_2 [20], mixed metal oxides such as perovskite [21], ferrites like $CuFe_2O_4$ [22], $CoFe_2O_4$ [23], and g-C_3N_4 [24] were developed and investigated for photocatalytic solar hydrogen production. All these investigations and other studies have proven that the structure of the active material significantly alters the efficiency of the water-splitting process. To improve the catalytic efficiency of this process, there is a lot of interest in the development of nanostructured catalysts or nanomaterials with high activity, rapid reactions, and good operational stability [25,26]. For example, photocatalytic materials with large surface areas, high crystallinity, small crystallite sizes, and porous structures exhibited enhanced photocatalytic performance as compared to nonporous and low surface areas [27]. The most critical factors influencing a nanomaterial's structural properties, including its shape, porosity, particle size, and specific surface area, are the chemical synthesis methods and circumstances employed during its development. Recently, many common synthesis routes such as the hydrothermal route [28], sol-gel method [29–32], precipitation method [33], solid-state reaction [34], template-assisted route [35], and deposition [36] (Fig. 2) [37] were applied to obtain diverse photocatalytic materials. These techniques generally allow for the design and manufacturing of nanostructures on a laboratory scale, but they frequently need difficult synthesis conditions, time-consuming operating steps, and slow reaction times, making them ineffective for practical mass production [38]. Comparison of different synthesis routes with material characteristics, equipment used, and limitations is provided in Table 1. Therefore, to further the commercialization of an improved energy conversion method, it is crucial to create straightforward, efficient, and economically feasible synthesis methodologies for the large-scale manufacturing of functional nanostructured materials.

Flame Spray Pyrolysis (FSP) is a very promising flame-based synthesis technology that has the potential to fulfill these demands. This method can be considered as a simple, rapid, scalable, and single-step fabrication technique that produces nanopowders [39]. These FSP-made powders have high surface areas, which is a necessary quality for applications in the paint and catalysis industries as well as additives in the rubber industry. They can be precisely tuned to produce particles ranging in size from a few nanometers to micrometers. This high-temperature in-situ synthesis of generally crystalline nanomaterials removes the need for several traditional pre- and post-treatment procedures like hydrothermal, sol-gel, and precipitation procedures and offers a viable platform for the scalable and affordable synthesis of nanomaterials with a consistent composition and distinct structural characteristics. In addition, FSP acts as an effective methodology for formation of the porous materials exhibiting high surface area and robust activity can be achieved using this technique owing to the quick evaporation of the liquid phase from the solution and breakdowns of the solute molecules. As the present article deals with the TiO_2-based materials fabricated via flame spray pyrolysis, this synthesis technology has been found beneficial in improving the catalytic activity of the synthesized materials. FSP-generated TiO_2 nanoparticles possess high surface area and good dispersion, which provides more active sites for catalytic reactions and make them easy to incorporate into the catalytic supports. Moreover, variation in the FSP parameters leads controlled crystallinity of the nanoparticles which helps in optimization of nanoparticles for specific catalytic applications. Even with these notable benefits, FSP has certain disadvantages that should be mentioned, such as challenges with producing multicomponent materials, hazardous gas reactants as a byproduct, and hard agglomerate formation in the gas phase that makes it difficult to produce high-quality bulk materials. Nevertheless, the benefits of the FSP technique have prompted a thorough investigation into the creation of the FSP reactor, which has revealed the influence of precursor chemistry on the end products' morphology and structure. Many recent review articles have provided summaries of these findings [40–42]. For example, Venkatesan et al. reviewed different nanomaterials and films fabricated using the FSP method and demonstrated their suitability for polymer electrolyte membrane fuel cells and solid oxide cells [43]. Chen et al. summarized transitional metal oxide films with designed functionalities fabricated by one-step FSP and investigated their suitability in electrochemical and photoelectrochemical water splitting [44].

To the best of our knowledge, no reports exist about the synthesis of TiO_2-based materials utilizing FSP and their use in various catalytic

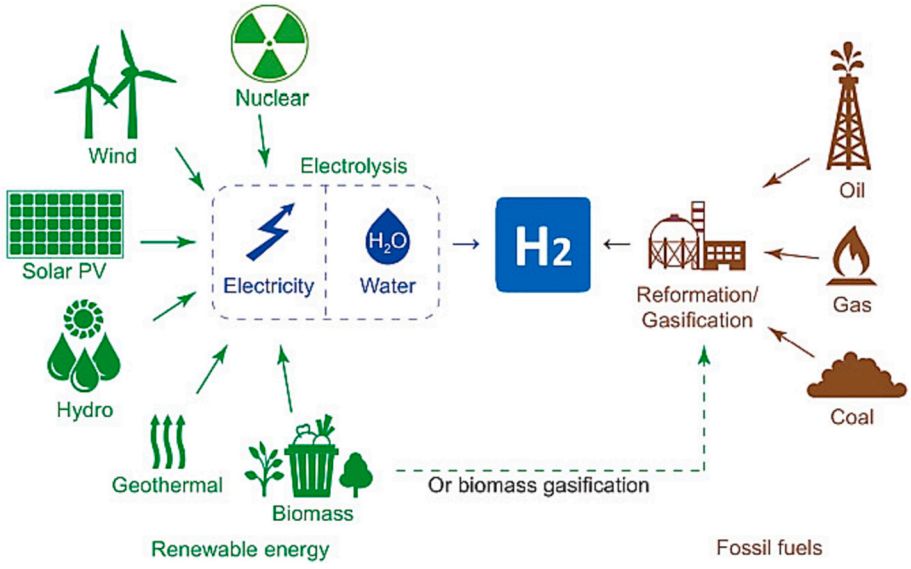

Fig. 1. Renewable and nonrenewable routes of hydrogen production [13].

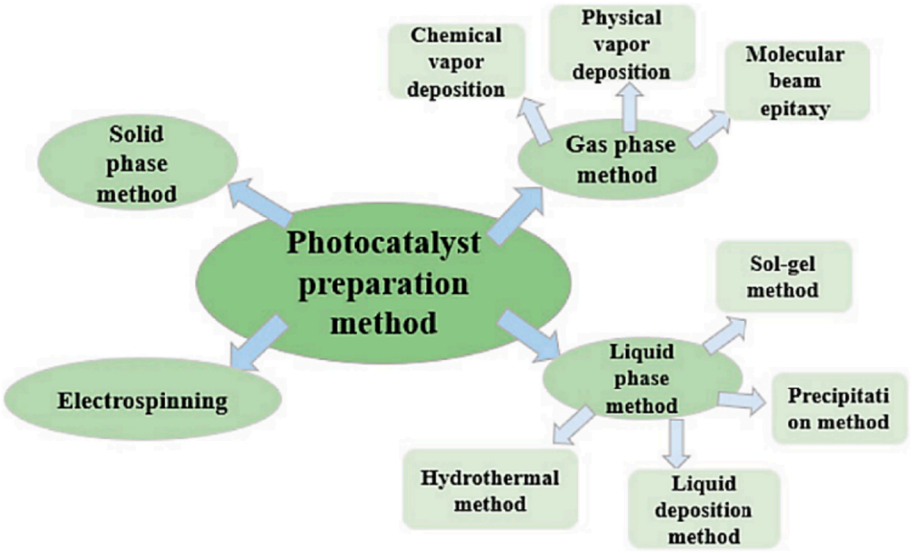

Fig. 2. Different methods for the synthesis of photocatalytic materials [37].

Table 1
Comparison of different synthesis methods for nanoparticles.

Synthesis method	Equipment	Product features	Technological process	Limitations
Hydrothermal	Autoclave	Uniform, controlled size and morphology	Simple and convenient	Expensive equipment
Precipitation	Beaker	High purity and controllable particle size	Easy and efficient	Long chemical reaction
Combustion	Vessel made up of graphite or aluminum plate	High porosity and purity	Rapid and simple	Limited materials types
Microwave assisted pyrolysis	Microwave chemical reactor	Uniform, pure, and narrow size distribution	Controlled and complex	Long reaction time and complex process
Solid-state reaction	Grinder, mixer, and furnace	Pure and homogeneous	Simple and scalable	Slow reaction rates and unwanted by-products
Spray pyrolysis technique	Atomizer and tubular furnace	Uniform and well-shaped nanoparticles	Controlled and complex	Insufficient smooth and flat film surface

applications. In this review, the foundational elements of the flame spray pyrolysis technology, including the equipment components, different types of FSP, and mechanism of particle formation through the FSP synthesis method were outlined in more depth. Then, the recent progress in the use of this technique in the preparation of TiO_2-based nanomaterials and their potential applications in catalysis (photocatalysis, thermocatalysis, and electrocatalysis) was discussed for the first time. Finally, this review is concluded by outlining our opinions on critical issues and potential development paths for FSP.

2. Flame spray pyrolysis (FSP) method

FSP, as a form of spray pyrolysis, emerged in the past few decades because of its ability to produce high-performance nanoparticles with different morphologies and varied crystallinity without post-treatment [45,46]. In addition, this synthesis methodology is a flexible technology in the flame synthesis family that, in addition to providing more flexible in terms of material selection and design as compared to conventional flame processes, gives additional design options [47,48]. Evonik-Degussa P25 is a well-recognized compound from flame-generated TiO_2 nanoparticles, which were employed as the primary component or test benchmark in various photocatalysis experiments [49]. According to research by Mädler et al., single-component, and multicomponent nanoparticles may be synthesized using the FSP technology with great purity and excellent dispersion [50]. Typically, during a flame spray pyrolysis process, the precursor solution is consistently supplied into a dual-fluid atomizing nozzle at a steady rate, where it is broken down into tiny droplets by pure oxygen dispersion gas moving at a high velocity. Then, a closely positioned annular pilot flame composed of a premixed mixture of CH_4-O_2 initiates combustion of the fine mist of small droplets, leading to the formation of a turbulent flame of elevated temperatures. In the subsequent pyrolysis and oxidation process, the metal salts undergo a transformation into metal oxides. These metal oxide monomers then undergo various stages of development, including nucleation, coagulation, and sintering, among others, eventually forming nanoparticles. Aerosol flame is then subsequently cooled down to normal temperature conditions by a cold sheath gas due to turbulence entrainment. Thereafter, a filtration system composed of a glass-microfiber is placed above the burner, resulting in the accumulation of the nanoparticles as powder, as illustrated in the Fig. 3 [51]. This makes FSP a quick, one-step process for catalyst production that can theoretically be expanded by the inclusion of more components [52]. Keep in mind that the formation of nanoparticles is a complex function of the synthesis procedure variables, including the profile of the material concentration distribution, the temperature distribution, and the flow characteristics in the high temperature environment.

The creation of tiny particles can benefit from this method in two keyways. Materials are first combined in a solution, which causes them to be initially uniformly combined at the atomic level. Second, the formation of crystalline particles merely requires sub-sintering temperatures. It enables the production of nanoparticles having diameters typically between 5 and 500 nm [53]. Additionally, makes it possible to create nanoparticles of significantly large specific surface areas. One of the major shortcomings of nanostructured films was their poor mechanical stability, despite their inexpensive production costs [54]. Controlling the concentration of the precursors, residence time in the system, and temperature near the flame are also necessary for

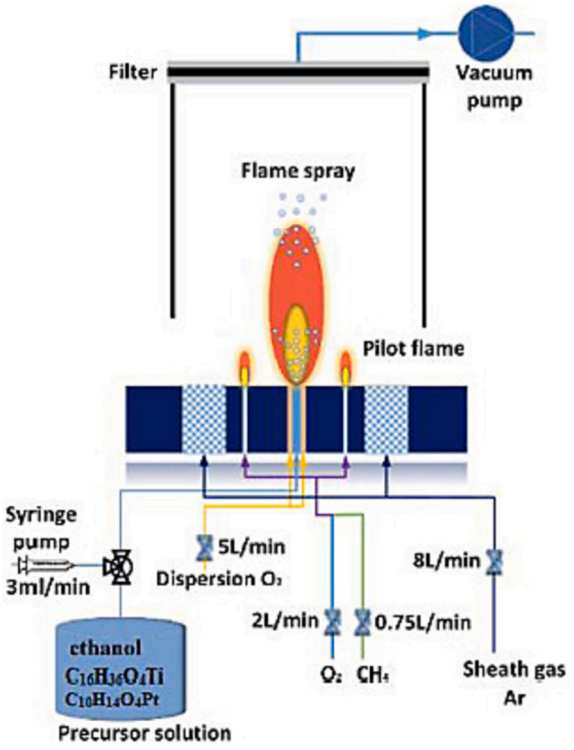

Fig. 3. Sketch for flame spray pyrolysis method [51].

monitoring the morphology [55]. Generally, a higher concentration of the precursors results in the formation of larger TiO_2 particles with spherical shapes. This is because the large amount of precursors facilitates particle growth and decrease the surface area-to-volume ratio, resulting in a more compact morphology. Higher flame temperatures typically result in the production of smaller TiO_2 nanoparticles with a more irregular shape. This is due to the increased energy input during FSP, which enhances particle nucleation and reduces particle growth time. The rapid solidification of nanoparticles at high temperatures can lead to imperfections in the crystal structure, resulting in a less regular morphology. Higher flow rates of carrier gas promote the rapid removal of reaction products from the flame zone, preventing particle agglomeration and favoring the formation of smaller TiO_2 nanoparticles with a more uniform shape. The increased gas flow also enhances the mixing of precursor droplets, leading to a more homogeneous distribution of nanoparticles. Numerous nanostructured metal oxides can be investigated via flame spray pyrolysis synthesis. Tricoli et al., and Wallace and his team used this method to synthesize ZnO nanoparticles [54,56]. While Phanichphant and his colleagues synthesized Nb-doped TiO_2 nanoparticles using this technique and were employed in ethanol sensors [57]. By carefully controlling FSP parameters and incorporating dopants or composite materials, the morphology and composition of TiO_2 nanoparticles can be tailored for specific applications. For instance, TiO_2 nanoparticles with a high surface area and a narrow band gap are suitable for visible-light photocatalysis, while TiO_2 nanoparticles with a controlled morphology and composition can be used in photoelectrochemical devices or sensors. Additionally, other metal oxides nanostructure like Al_2O_3, V_2O_5, Fe_2O_3, ZrO_2, WO_3, SnO_2 or Mn_2O_3, were also fabricated utilizing the flame pyrolysis method [58–63]. Another important advantage of employing this technique of synthesis is the availability of cheap metal precursors that may be mixed during synthesis, leading to an endless variety of arrangements of metal ions and their stoichiometric ratios. Complex and mixed oxide synthesis is made possible by applying this method. Composites like WO_3/ZnO and WO_3/TiO_2 have been reported that described the use of FSP approach for the fabrication of nanocomposite structures [64,65].

2.1. Types of FSP

Three types of flame spray pyrolysis have been identified: Liquid-fed aerosol flame synthesis (LAFS), Vapor-fed aerosol flame synthesis (VAFS), and flame-assisted spray pyrolysis (FASP) as shown in Fig. 4 [66]. In VAFS, the volatile precursors are hydrolyzed or combusted in a hydrogen, hydrocarbon, or halide flame [67]. Particles are created during nucleation from a precursor's gaseous phase, and they grow through surface reactivity and/or coagulation before coalescing into bigger particles. For that reason, this process is frequently employed on an industrial scale to produce pigmentary titania, waveguide preforms, alumina, and fumed silica [68–70]. Nevertheless, VAFS is only applicable to a small number of materials, though, due to the reasonably priced availability of volatile precursors. Since non-volatile precursors can be given, liquid-fed aerosol flame synthesis is significantly more flexible. LAFS, often known as the “furnace process,” is used to generate carbon black [71]. Typically, the product is created by spraying an emulsion, slurry, or liquid precursor solution. When droplet evaporation is not fully accomplished, it leads to the formation of hollow and shell-like particles at the micron scale. Conversely, complete evaporation of the precursor results in the production of solid nanoparticles, as exemplified in VAFS.

The spraying process involves atomizing the solution using either air-assist or ultrasonic nozzles, while an external heat source facilitates the evaporation of the precursor. In the case of a combustible organic solution with a high enthalpy content nearly >50% of the total combustion energy, a relatively small pilot flame is employed to ignite and maintain the combustion of the spray. This procedure is commonly referred to as flame spray pyrolysis (FSP), as depicted in Fig. 4. Conversely, an external hydrogen or hydrocarbon flame is needed to help with the burning of an aqueous spray solution of inorganic precursors that possess a low enthalpy content (50% of the total combustion energy). This approach is commonly referred to as “flame-assisted spray pyrolysis” (FASP). Advantages and disadvantages of all these three types of processes are presented in Table 2 [72]. Among these pyrolysis methods, FSP is the youngest and the focus of this review, offering significant technological features like self-sustaining flames, utilization of liquid feeds and less volatile precursors, demonstrated scalability, generation of high-temperature flames, and the occurrence of substantial temperature gradients. Flame spray pyrolysis has therefore emerged as a practical technique for the efficient, rapid, and one-step synthesis of both single and multicomponent nanoparticles on both laboratory and industrial scales. These intricate and functional nanostructures created by the FSP approach have found use in several significant fields, including catalysis (as reviewed by Strobel et al.) [73], optics and photonics [74], sensors [75], health care [76], magnetic materials [77], electroceramics for fuel cells [78] and composite materials [79]. Even though FSP research is just getting started, the applications for such nanomaterials are so promising that early FSP start-ups are already up and running. Recent announcements from Johnson Matthey Co., a significant catalyst manufacturer, mention systematic investigation of FSP-synthesized catalysts at its Research Center in the UK [80]. Both in particle design and applications, there are still many things to learn. Continuing multidisciplinary information exchange across materials science, aerosol technology, and combustion engineering is essential. Every new materials system inevitably has a certain level of complexity.

2.2. Mechanism of particle formation in FSP

In the FSP process, two distinct pathways for particle production have been identified. One is the conversion of gas into particles. Homogeneous particle production in FSP occurs when the precursor is fully vaporized within the flame, subsequently undergoing conversion in the gas phase [81]. The other is the conversion of droplets to particles. Large, dense, or hollow nanoparticles are produced when the precursor is not completely vaporized, precipitating, and converting within the

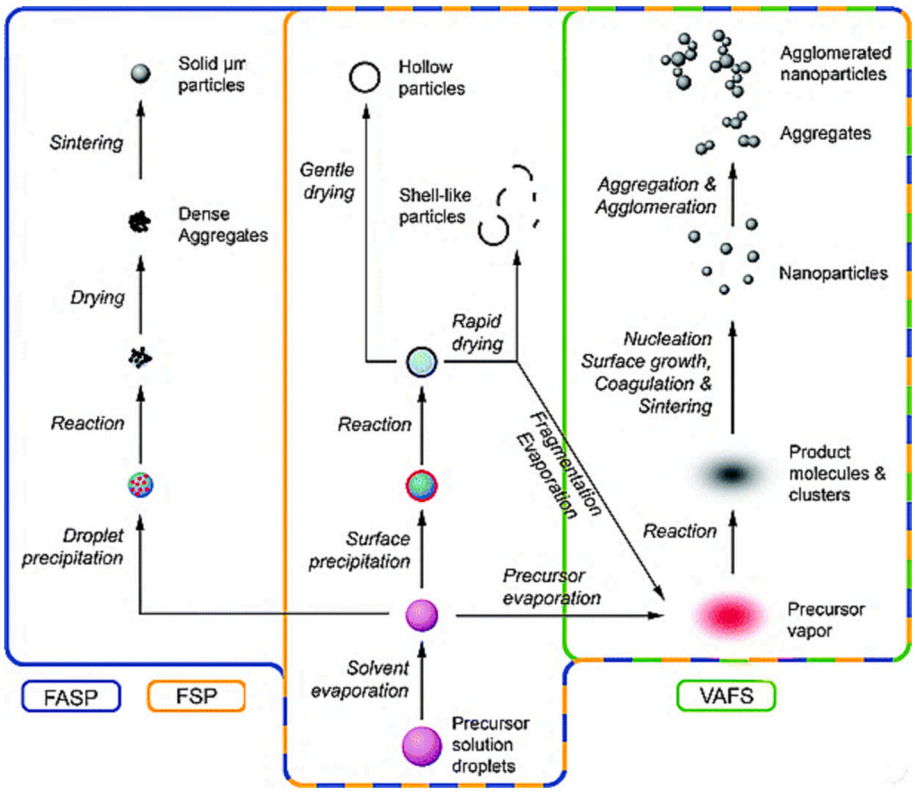

Fig. 4. Types of flame spray pyrolysis (FSP) [66].

Table 2
Advantages and disadvantages of Liquid-fed aerosol flame synthesis (LAFS), Vapor-fed aerosol flame synthesis (VAFS), and flame-assisted spray pyrolysis (FASP).

Synthesis process	Advantages	Disadvantages
Liquid-fed aerosol flame synthesis (LAFS)	Wide range of liquid precursors offers versatility in synthesis Controlled particle size due to liquid precursor atomization process Homogeneous coating due to controlled precursor atomization	Complexity due to precise control over atomization and combustion conditions Limited scalability Limited residence time in flame may affect the uniformity and quality of the material
Vapor-fed aerosol flame synthesis (VAFS)	Easier to handle and vaporize High purity of the synthesized material Higher scalability	Limited precursor options Limited range of materials can be synthesized Complex vaporization in certain precursors can be technically challenging Achieving homogeneity in particle size and distribution might be more challenging as compared to LAFS
Flame-assisted spray pyrolysis (FASP)	Utilization of both liquid and vapor phase precursors Offers better control over particle morphology and structure Easier to scale up as compared to other methods	Complex due to the need for precise control over spray parameters and combustion conditions Requires specialized equipment for precise spray and combustion control Ensuring uniformity in large-scale production might be challenging

spray droplets [82] As shown in Fig. 5 [73,83].

For the synthesis of ceramic powders and films, either technique is appropriate. However, due to its greater application, most recent and

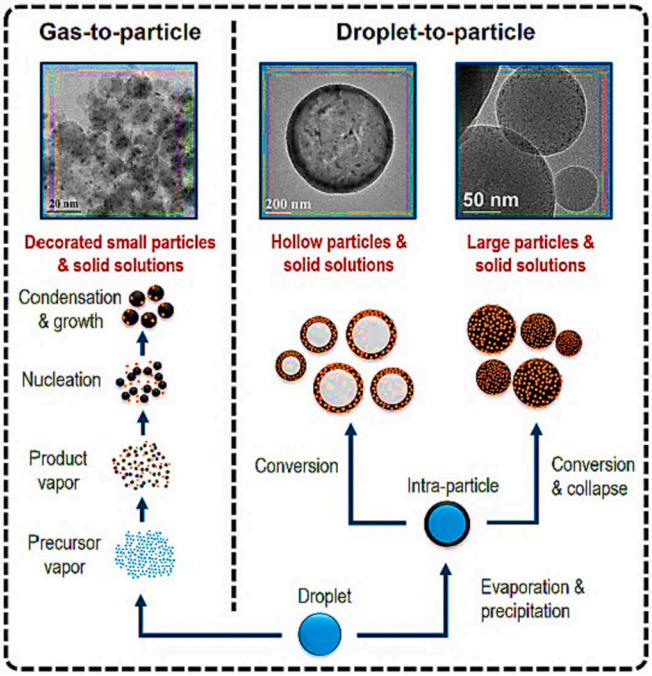

Fig. 5. The particle production paths in the FSP process [73,83].

earlier research papers advocate for the first approach for obtaining homogenous particles [84]. Evaporation of droplets and combustion processes, which influence precursor combustion and particle nucleation, are fundamentally important to this aim and must be understood. However, conducting experimental studies in flame spray pyrolysis poses several challenges due to various factors. These include the

interaction between droplets, the high temperature of the flame, significant temperature variations within the system, turbulence resulting from droplet dispersion, and the limited time available for observation due to the rapid nature of the process. Jossen and his team suggested two criteria in order to examine the conversion routes in FSP: (1) the ratio of solvent boiling temperature to the precursor decomposition temperature and (2) combustion enthalpy density [85]. Later, Strobel and Pratsinis examined the impacts of solvent composition in the gas-to-particle conversion process using metal nitrates as precursors. They discovered that the addition of liquid 2-ethylhexanoic acid (2-EHA) to the solvent had a significant impact on improving the conversion efficiency [158]. According to research by Wei et al. [86] on droplet behavior using various solvent compositions, the addition of 2-EHA may be able to convert nitrates into low-boiling 2-ethylhexanates because of the ligand exchange effect. Another research group used rainbow refractometry to observe the combustion behavior of a single 100 ml droplet, and through their observations, they subsequently proposed a microexplosion process for multicomponent liquid droplets [87]. Furthermore, Meierhofer et al. [88] employed a single droplet combustion study to analyze the presence of multimodal particle sizes and phase impurities resulting from undesirable droplet-to-particle conversion routes. Their research focused on the analysis of various precursor solutions for $Li_4Ti_5O_{12}$ as energy storage material. It was found that flame extinction and partial vaporization of the precursors result in the formation of residuals during single droplet combustion. These residuals were found to be responsible for the development of inhomogeneous particles. However, they observed that by replacing ethanol with 2-ethylhexanoic acid (2-EHA) as the solvent, the incidence of residuals could be reduced, leading to enhanced vaporization and the production of homogeneous particles. Furthermore, the researchers found that the particles generated through FSP, and single droplet combustion exhibited identical characteristics in terms of crystalline size, state, and phase purity. Their finding supported the idea that single droplet combustion could serve as a predictive tool for assessing product quality, interpreting particle formation, and driving improvements in the generation of homogeneous nanoparticles through FSP. Additionally, FSP's simulation of particle formation recently utilized experimental data obtained from single droplet combustion [89]. Despite these promising findings in analyzing the mechanisms, and applications of the obtained particles in different fields, investigations related to the synthesis of TiO_2-based materials by the FSP for photocatalytic and catalytic applications are still missing, so more in-depth information must be learned. Thus, the goal of the current work is to close this gap by conducting a thorough analysis of how the FSP method contributes to the generation of nanoparticles for different photocatalytic and catalytic applications. Another specialized version of flame spray is flame jet pyrolysis in which the precursor solution is atomized into very fine droplets. These droplets are then injected into a high-velocity gas stream, which accelerates them into a hot flame. The rapid acceleration of the droplets helps to break them down into even smaller nanoparticles.

3. Catalytic applications of TiO_2-based materials synthesized by the FSP

3.1. Photocatalysis

3.1.1. Photocatalytic hydrogen production via water splitting

Photocatalytic water splitting to produce hydrogen has garnered a lot of interest as a possible source of renewable energy with no dependency on fossil fuels and no emissions of carbon dioxide. As illustrated in Fig. 6a [90], the process consists of three main steps; (i) photon absorption by photocatalyst which leads to the generation of negative electrons in the conduction band and positive holes in the valence band of the semiconductor, (ii) charge separation and migration to surface to initiate the redox reaction, and (iii) surface chemical reaction between the generated carriers and water to produce hydrogen and oxygen. Recently, several oxides and mixed metal oxides including perovskites and many doped oxides were tested for photocatalytic water splitting [90]. Nevertheless, titanium dioxide (TiO_2) is still the best photocatalyst due to its high activity, high efficiency and stability, biocompatibility, appropriate band positions, chemical inertness, affordability, and non-toxicity [91]. The molecular orbital diagram (Fig. 6) depicts the interactions between Ti and O atoms in TiO_2 [92]. The bonding and antibonding orbitals are primarily made up of the “d” orbitals of Ti and the “p” orbitals of O [93]. Bandgap energy (*Eg*) is the amount of energy that separates the lowest unoccupied molecular orbital i.e. (CB) from the highest occupied molecular orbital i.e. (VB). An energy gap of roughly 3.2 eV is present in the TiO_2 anatase. Because of its large band gap energy, TiO_2 can only be excited by UV light, which reduces the efficiency of solar to hydrogen energy (STH) conversion [94]. Numerous TiO_2 modification techniques, including anion doping, metal ion doping, semiconductor materials, and others, have emerged to increase solar absorption and increase STH efficiency [95]. Among these, the oxide surface modification of non-noble metals like copper or nickel combined with the deposition of noble metal nanoparticles (Au, Pt, Ag) has resulted in a notable improvement in photocatalytic activity and efficiency in solar light exploitation. Flame spray pyrolysis (FSP) was found to be a successful process for creating nanosized TiO_2 and TiO_2 modified with noble metals, producing materials with high surface areas, anatase contents, crystallinity, and excellent noble metal dispersion [96]. As a result, the obtained catalytic materials have excellent performance due to the enhanced charge separation efficiency and reduced charge recombination rate. Therefore, a combined TiO_2 catalyst synthesized by the FSP with noble or non-noble metal modification can be considered an outstanding method to improve the catalytic performance. Moreover, it has recently been demonstrated that a TiO_2 photocatalyst made using FSP is more effective than Degussa P25 in photomineralizing saccharides [97].

Chiarello et al. produced a variety of TiO_2 and TiO_2 that had been treated with gold using flame spray pyrolysis, and they then tested their photocatalytic activity both for the overall water-splitting reaction and

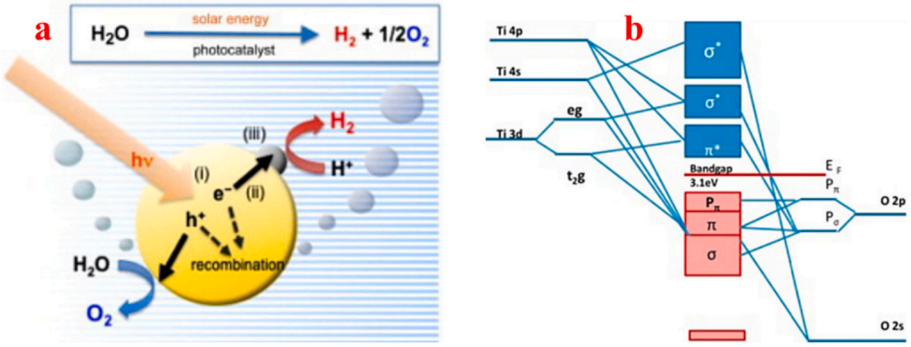

Fig. 6. Schematic illustration of water splitting over photocatalyst (a) [90], and molecular orbital diagram of TiO_2 (b) [92].

for methanol-assisted water splitting [98]. Their findings demonstrated that as the anatase concentration rose, so did the photocatalytic activity. Additionally, by modifying the FSP parameters, the solvent, photocatalyst surface area, and crystallinity are primarily improved, resulting in an improvement in photocatalytic performance. Additionally, FSP-synthesized TiO_2 from a xylene solution and containing 1% Au exhibited the highest activity (8 mmol of H_2/h/g of the catalyst) compared to P25. The same research group also synthesized TiO_2 and 1%Au-TiO_2 with high surface area by FSP and the resultant product was examined for photocatalytic hydrogen production via steam photoreforming of methanol [99]. An important finding of this study is that the activity of the obtained photocatalytic powder is significantly influenced by the type of reactor used and showed that the vapor phase photoreactor enhanced the hydrogen production activity up to 10.2 mmol of H_2/h/g of catalyst, conforming to a 6.3% apparent photon efficiency. Recently, Gao and his colleagues synthesized a batch of Pt/TiO_2 catalysts via FSP to assess their photocatalytic hydrogen generation capability [51]. The most active catalysts among these ones were those with a 0.1% molar ratio of platinum to TiO_2 (Fig. 7a&b). This enhanced activity can be accredited to the presence of single Pt atoms, which act as the primary active sites for photocatalytic hydrogen evolution. Additionally, Fig. 7c shows that the desorption temperature of H_2 is lower for TiO_2 (without Pt), and the hydrogen desorption peak is higher on the Pt-loaded TiO_2. These observations indicate that the Pt atoms enhance the dissociation of H_2 molecules and facilitate the movement of H^+ species towards the TiO_2 surface. As a result, the amount of hydrogen that can be adsorbed by the catalyst increases. Moreover, Pt fosters the reverse hydrogen overflow from TiO_2 to Pt during the desorption process, which raises the quantity of H_2 that is absorbed and lowers the desorption temperature. To put it another way, H^+ may be transferred to the Pt atoms more easily and participate in the photocatalytic H_2 production reaction. Upon absorption of photoelectrons from TiO_2 and create adsorbed H atoms. These H atoms subsequently bind together to form H_2 molecules through reactions facilitated by Pt as an active site. Finally, the formed hydrogen molecules desorb from the catalyst surface. In conclusion, it is hypothesized that the presence of Pt in the TiO_2 catalyst plays a dual role in enhancing hydrogen production activity. Firstly, Pt promotes the separation of electron-hole pairs, thus increasing the efficiency of charge utilization in the photocatalytic process. Secondly, Pt facilitates the transfer of hydrogen to its surface, leading to the formation of hydrogen molecules through reverse hydrogen spillover. This combined effect of Pt accelerates the overall hydrogen production process and contributes to the enhanced activity observed.

Bernareggi et al. coupled TiO_2 with transition metal Cu and noble metal Pt to increase its photocatalytic hydrogen production efficiency through photoreforming of methanol [100]. Two series of modified TiO_2 photocatalysts were prepared using one-step flame spray pyrolysis, the first group contains only copper with different weight ratios, whereas the second group contains both copper and platinum. The remarkable hydrogen production activity was observed with the material that has Pt and 0.5% wt Cu. A synergistic effect between these two metals deposited over TiO_2 was responsible for the enhanced photocatalytic activity of TiO_2 compared to a single metal-modified titania. Noble metals such as Pt and Au have a significant impact on improving TiO_2's photocatalytic activity for producing hydrogen, but their expensive cost limits their use in photocatalysis and requires the researcher to look for alternatives. As a result, transition metal doping might be viewed as a viable method to increase TiO_2's charge separation efficiency and produce visible light activity [101]. Hence, the procedure of doping, as well as the concentration and nature of dopant atoms, are only a few of the variables that affect how doping affects an activity [102]. For example, the band-gap energy can be decreased by doping or introducing transition metal ions like Fe, and Cu into TiO_2, shifting the absorption spectra towards the visible light area [103]. Additionally, these transition metal ions also act as locations for shallow charge trapping, which lowers the rate of electron-hole recombination. Copper (Cu) has been considered as being

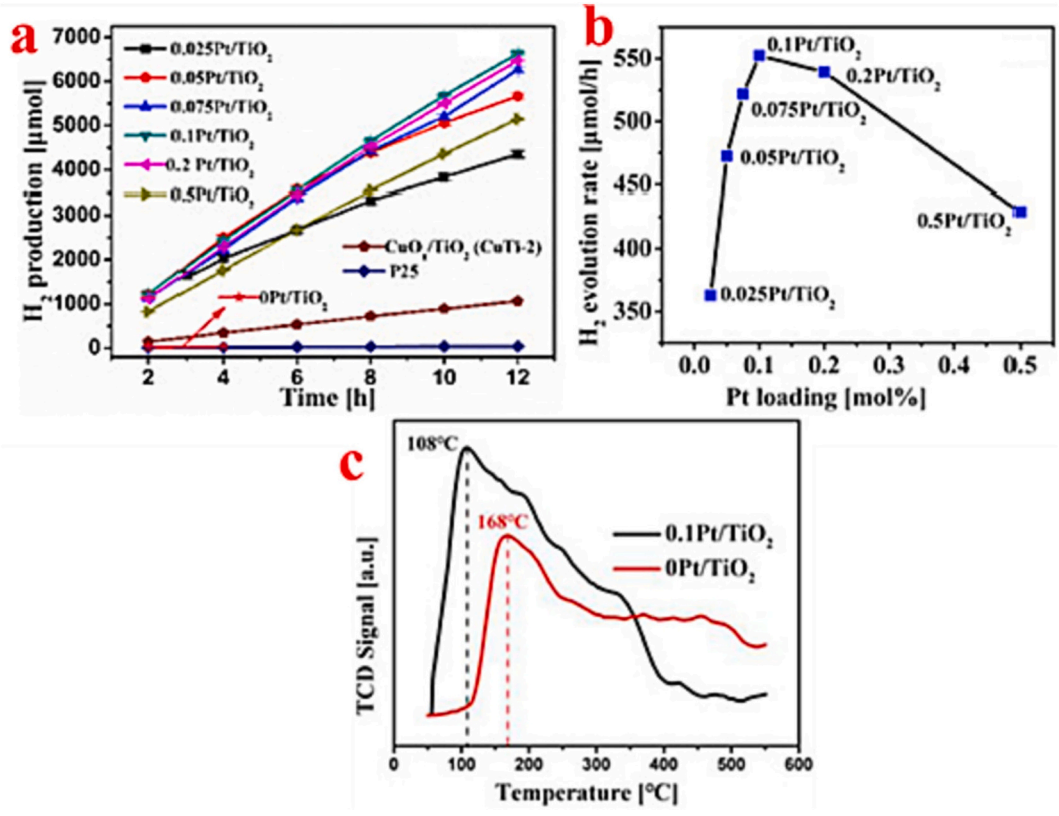

Fig. 7. Photocatalytic hydrogen production activity of different Pt-loaded TiO_2 catalysts (a&b), and the hydrogen temperature-programmed desorption (H_2-TPD) profiles of 0.1Pt/TiO_2 and pure TiO_2 (c) [51].

significant among the different elements doped into TiO_2 thus far due to small energy bandgap of its oxides (Cu_2O has 2.2 eV and CuO has 1.4 eV) and their strong light absorption coefficients [104]. Additionally, it has been demonstrated that copper surface cluster modification is an effective method for enhancing charge separation [105]. For instance, Yang and his team prepared a high-efficiency hybrid CuO_x/TiO_2 photocatalysts via a one-step flame spray pyrolysis approach. The fabricated composite material was then tested for photocatalytic hydrogen generation under Xe irradiations in the presence of methanol [106]. The hydrogen production achieved was 112.6 μmol h^{-1}, which is around 22 times greater than the commercial P25. According to the authors, density functional theory simulations and photoluminescence spectra provide valuable insights into the mechanisms behind the enhanced photocatalytic properties. It is observed that there are two significant factors involved (1) bulk defect levels and (2) surface deposited CuO_x nanoclusters. These defects are essential for charge separation and deposition of CuO_x nanoclusters extend the spectrum responsiveness. The process of fluorination, which can involve either surface modification (adsorption of fluoride anions) or lattice fluorine doping, is considered one of the methods used to increase the photocatalytic efficiency of TiO_2. Surface fluorination is simply an exchange reaction between surface hydroxyl groups and fluoride anions. As a result, chemical properties of titanium dioxide's surface and photoactivity—which is also highly dependent on the reaction substrate-undergo considerable changes [107]. On the other hand, doping occurs when fluorine actively aids in the crystallization of TiO_2, altering its size, shape, phase, crystallinity, and exposed facets as well as altering the organization of crystal into peculiar topologies and pore architectures [108]. Chiarello and his colleagues synthesized fluorinated Pt/TiO_2 photocatalysts utilizing single-step FSP and tested for photocatalytic H_2 production through the photoreforming of methane (Fig. 8a) [109]. Tests on photocatalytic hydrogen synthesis revealed that the replacement of 5 at.% F atoms for O atoms in TiO_2 increased the H_2 and CO_2 generation rates (Fig. 8b). However, at higher F concentrations from this level, the formation rate of H_2 declined linearly with increase in the nominal loading in the material. XPS tests indicated the existence of both bulk and surface fluorine. According to XAS analysis, Pt was largely supported in the oxidized form, as the materials were created and it reduced quickly into the metallic form in the presence of gas-phase reaction conditions, where it subsequently functioned as an electron sink to draw electrons and improve the charge separation efficiency (Fig. 8c). Furthermore, due to the F-induced surface electronegativity, structural defects are introduced owing to the excessive fluorination that in turn serve as recombination sites for electron-holes and may impede interface electron transport. Both effects work together to reduce photoactivity.

3.1.2. *Photocatalytic degradation of organic pollutants*

The manufacture of textiles, paint, and leather results in the release of several organic pollutants into water bodies. These organic effluents might significantly harm aquatic ecosystems and human health since they are extremely difficult for nature to decompose or eliminate [110]. The treatment of wastewater has been proposed using several standard techniques, including membrane filtration, chemical precipitation, adsorption, and biological treatments. These strategies might not, however, always be practical or very effective [111]. For example, in biological treatment, several studies have also shown that microalgae may be grown for use in wastewater treatment. However, while employing microalgae, the contaminated effluents are often required to

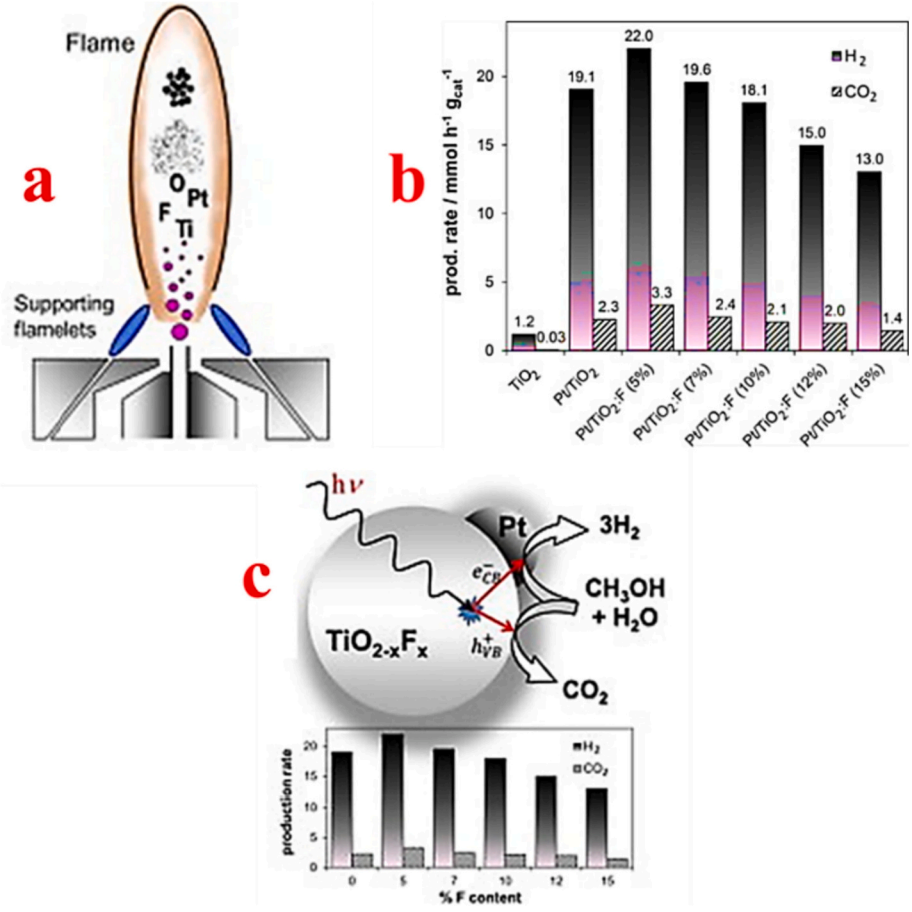

Fig. 8. A sketch for the flame spray pyrolysis used for the photocatalyst synthesis (a), the hydrogen production rate (b), and the mechanism of H_2 production over a series of F-substituted TiO_2 photocatalysts (c) [51].

be in much diluted state before biological treatments. Prior to introducing green algae, waste effluent may be diluted up to five times with the synthetic media to minimize toxicity because microalgae are sensitive to concentrated toxicity. Additionally, biological processes are extremely difficult to manage due to the variable content and volume of wastewater. Operators need to control these changes [112]. On the other hand, however, some organic effluent still not impressively degrade through biodegradation. Although chemical precipitation is frequently used to remove organic pollutants from wastewater, it still has several drawbacks. For example, it uses a lot of chemicals, necessitates physical-chemical testing of the effluent, produces a lot of sludge, and occasionally results in secondary pollution [113]. For membrane filtration, most commercial membranes are not regarded as semi-permeable. Thus, they are not able to restrict small, non-charged, and low molecular weight organic solutes [114]. In addition, low flow rates or limited throughput caused by clogging or fouling issues may also limit some applications for membrane separations when pollutant concentrations are higher. Adsorption procedures and photocatalytic degradation reactions are now considered to be the prime methods for decontamination of polluted water and air [115]. Though, adsorption does not actually remove contaminants; rather, it only moves them from one phase to another and reduces their concentration [116]. On the other side, photocatalysis can be considered a promising approach to the degradation and conversion of different organic molecules into CO_2 and H_2O using solar energy and nontoxic, and efficient photocatalysts without secondary pollution [117]. The degradation process requires the same steps as in photocatalytic hydrogen production, the only difference is instead of the generated electrons and holes initiating the hydrogen and oxygen production in water splitting reaction, herein, electrons produced in the CB reduce oxygen to superoxide radicals, and the holes oxidize the adsorbed hydroxyl anions to hydroxyl radicals, which form the main active species responsible for the degradation reaction (Fig. 9a) [118]. Currently, TiO_2 photocatalyst which is synthesized by different routes is widely used to degrade organic pollutants in both liquid and gas media [119]. Thus, the capacity to modify its structural characteristics during the synthesis stage is essential for optimizing it in view of practical technological applications [120]. Due to various benefits including low cost, ease of operation and experimental setup, capability for mass production, ease of doping, reproducibility, and quick particle growth, the FSP is an appealing, adaptable, and useful approach to manufacturing TiO_2 nanoparticles. As already mentioned, the principle of FSP procedures is the exothermic burning of a precursor spray of an organic liquid and can produce crystalline nanoparticles without the need for additional post-production heat treatment. Bettini and his team studied the impact of the FSP operation conditions on the properties and photocatalytic activity of nanostructured TiO_2 [121]. Results showed that an increase in the molar ratio of the dispersion O_2 gas and the titanium (IV) isopropoxide (TTIP), resulted in decreasing the particle size and enlarging the specific surface area, leading to enhanced photocatalytic activity of TiO_2 powder in the decomposition of the formic acid in aqueous suspension. It is widely acknowledged that altering TiO_2 by adding non-metal or metal/metal oxide cations can force its visible light photocatalytic performance [122]. However, there are some disadvantages to the former route, including poor thermal stability, increased charge carrier recombination, and utilization of expensive metals and metal oxides [123]. For these reasons, modification of TiO_2 with non-metals like S, N, or P has gained a lot of attention in forcing its photocatalytic properties. Among the various non-metal incorporated TiO_2, sulfur (S) has accomplished significant attraction because of high thermal stability and its ability to decrease the band gap energy of TiO_2. Boningari and his colleagues applied one step FSP method to fabricate visible-light S-doped TiO_2 photocatalysts [124]. The authors proposed a model of particle formation through flame spray pyrolysis and illustrated in Fig. 9b. The prepared S-doped TiO_2 photocatalysts were subjected to testing to evaluate their photocatalytic activity in the removal of acetaldehyde. According

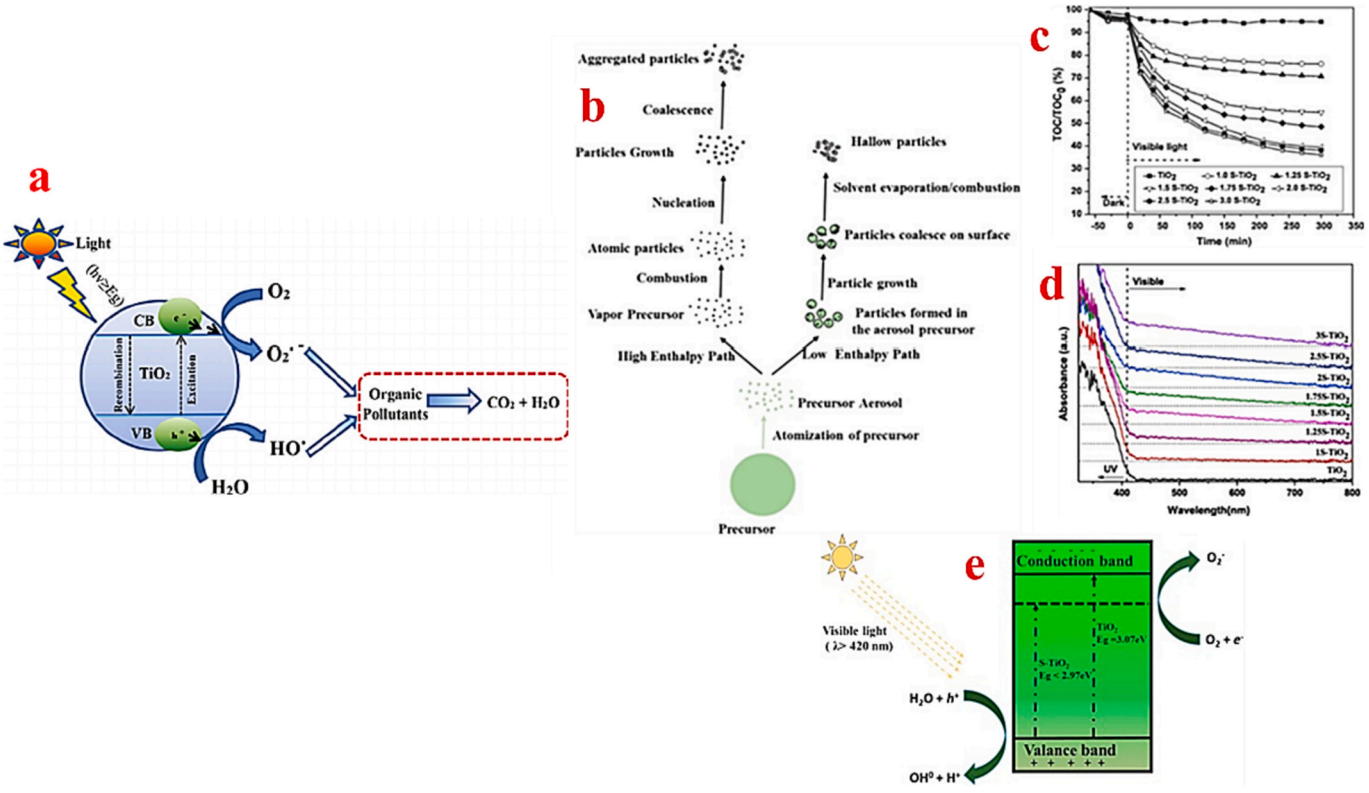

Fig. 9. Mechanism of organic pollutants degradation over TiO_2 under light irradiation (a) [118], model representing the synthesis and growth of particles in FSP (b), the time course photocatalytic conversion of acetaldehyde (c), UV–vis DRS spectra over TiO_2 and M S-TiO_2 (where M is the molar concentration of H_2SO_4 taken as S source in the precursor) (d), and mechanism of photocatalytic conversion of acetaldehyde over S-TiO_2 photocatalyst (e) [124].

to the XPS results, sulfur has two oxidation states, S^{4+} and S^{6+}. Among all prepared samples, 2S-TiO_2 exhibited remarkable efficiency for visible light-induced photocatalysis (Fig. 9c). This remarkably photocatalytic activity was mainly attributed to the high S^{6+} content in the 2S-TiO_2 that can reduce its band gap energy compared to pure TiO_2 (Fig. 9d&e).

In addition to sulfur, nitrogen (N) is also considered to be the most effective dopant due to its similar size to that of oxygen atom and its ability to create metastable defect complexes that stimulate the formation of electron-hole pairs [125]. Furthermore, doping with nitrogen can change the crystal lattice of the pristine TiO_2, and therefore decrease the recombination process between charge carriers, resulting in enhanced visible light activity compared to the undoped TiO_2. Thus, the synergistic interactions of numerous elements, including morphology, dominating facets, optical response, crystal phase, defects, and N- doping into TiO_2, are thought to be the cause of the improved photocatalytic activity under solar irradiation of N-doped TiO_2 [126,127]. Huo et al. recently described how to manufacture near-surface N-doped TiO_2 using the FSP process. However, this procedure consists of two-stages in which first involves the surface of TiO_2 modified by ammonia water while in the second phase it was created using the flame spray approach [128]. Their research showed that nitrogen may be added to TiO_2 nanocrystalline to lower band gap energy as well as increase the charge separation capacity. Smirniotis and his co-workers successfully synthesized N-doped TiO_2 with the help of a single-step flame aerosol method [129]. Their investigations showed that nitrogen was successfully incorporated into the TiO_2 crystal lattice in the N-doped TiO_2 catalysts, primarily as interstitial nitrogen rather than in the substitutional form. This type of incorporation was revealed by the shifting of (101) plane anatase diffraction peaks towards lower angles. The increased photocatalytic activity of this novel N-doped TiO_2 catalyst for degradation of phenol under visible light irradiation was mainly ascribed to the decreased band gap energy and improved charge separation as compared to pristine TiO_2. In a similar vein, metal doping, or doping TiO_2 with transition elements like V, Fe, Co, Mo, and Cr, can be thought of as a successful strategy to increase TiO_2's visible light activity [130]. Addition of transition metal ions to the TiO_2 crystal lattice can change the features of the material's electrons, improving its capacity to absorb visible light [131]. Recently, several methods were applied to synthesize transition metal doped TiO_2 like sol-gel, coprecipitation, liquid phase deposition, wet impregnation, and ion-implantation method. Nevertheless, these methods possess several disadvantages, for example, coprecipitation and sol-gel methods need additional heat treatments to achieve crystallization in the material. However, the post-treatment at high temperatures and the prolonged heating could cause the dopant metal ions to separate into their corresponding metal oxides. These metal oxides may serve as a site for recombination of electron-hole pairs, which would reduce the activity of photocatalysis [132]. For the wet impregnation method, it is improbable that metal ions will replace oxygen in bulk TiO_2 crystals, it may only happen over the surface [133]. Liquid phase deposition often requires a lengthy aging period to achieve optimal results and specific volume of sample. The drawback of the ion implantation procedure is that it requires complex and expensive facilities. Thus, applying a flame spray pyrolysis (FSP) approach in synthesizing transition metal doped TiO_2 can be a promising alternative to these conventional methods. Tian and his team synthesized V-doped TiO_2 photocatalysts via FSP and tested their ability for photodegradation of 2, 4 dichlorophenol and methylene blue dye [134]. Their findings demonstrated the successful incorporation of V^{4+} ions into the crystal lattice of TiO_2, resulting in enhancing the photocatalytic activity of TiO_2 in both UV and visible regions. The proper radius and energy level of chromium ions (Cr^{3+}) make them a prime contender to dope TiO_2 since the Cr^{3+} radius (0.755 nm) being quite near to that of the Ti^{4+} (0.745 nm) [135]. Additionally, the lattice of TiO_2 is readily capable of introducing Cr^{3+} ions. Also, there is a band gap of approximately 2.7 eV between the Cr^{3+} level and the TiO_2 conduction band [136]. This is advantageous due to more absorption of visible light by Cr-TiO_2. Same research group also reported a synthesis of Cr-doped bicrystalline TiO_2 nanoparticles with rutile and anatase phases by the flame spray pyrolysis method and examined their photocatalytic behavior towards of 2,4 dichlorophenol under visible light [137]. Highest degradation activity was exhibited by the 1% Cr-doped TiO_2 (Fig. 10a). This is not only because of the increased visible light efficiency (Fig. 10b) but also to the increased rutile contents in the photocatalyst (Fig. 10c&d). XPS measurements show that Cr^{3+} may effectively help to create oxygen vacancies, which helps to convert anatase into rutile (Fig. 10e). EPR study have revealed a strong correlation between the state of Cr ion in the material Cr-TiO_2 and the concentration of Cr within the material. Lower Cr content i.e. below 1%, it is mostly absorbed into the crystal lattice of TiO_2, whereas a greater content is beneficial for the production of Cr_2O_3 clusters. Finally, the presence of both phases (rutile and anatase) of TiO_2 as well as the formation of both superoxide and hydroxyl radicals are believed to be helpful for the effective photodegradation reaction of Cr-doped TiO_2 (Fig. 10f). Recent years have seen a quick increase in interest in Nb-doped TiO_2 because of its potential uses in sensors, dye-sensitized solar cells, and transparent conductive films [138]. Furthermore, the ionic radius of Nb^{5+} is slightly larger than that of Ti^{4+}, hence, Nb^{5+} can be easily doped into the crystal lattice of TiO_2 [139].

In order to accommodate the higher charge of Nb^{5+} when substituting for Ti^{4+} in the crystal lattice of TiO_2, two possible scenarios can occur, depending on the specific synthesis conditions. First, one Ti cation vacancy may be introduced for every four Nb ions incorporated. Second, a stoichiometric reduction of Ti^{4+} to Ti^{3+} may occur for each Nb ion introduced. These adjustments help to maintain charge balance within the crystal lattice [140]. In either case, these modifications can lead to the creation of donor levels located just below the conduction band (CB) edge of TiO_2 [141]. As a result, presence of these levels enables electronic transitions from the VB to these donor levels upon absorption of visible light, making the Nb-doped TiO_2, an active visible light photocatalyst. The photocatalytic activity for the oxidative destruction of organics is reduced when TiO_2 is doped with a significant quantity (>5 mol%) of Nb at the Ti site, according to previous research [142]. One possibility for the suppressed photocatalysis is that Ti vacancies are produced to balance out the increased positive charge on Ti^{4+} replacement with Nb^{5+}, even if the precise process is yet unclear. This is because emptiness typically functions as a center of charge recombination [143]. Saito et al. synthesized Nb-doped TiO_2 utilizing liquid-feed flame spray pyrolysis as the synthesis technique and subsequently subjected to NH_3 annealing [144]. The catalytic efficiency of the fabricated photocatalyst was investigated by the oxidative degradation of formic acid to CO_2 under simulated solar irradiations. According to the authors, the oxygen vacancy is produced at greater Nb concentrations during NH_3 annealing and is what prevents Nb-doped TiO_2 from being as photocatalytically active as pure TiO_2. Jiang et al. successfully prepared pristine and Cu, and F-doped TiO_2 using a FSP approach and checked their activity for photooxidation of acetaldehyde [145]. Although both Cu and F-doped TiO_2 have the same elemental states according to the XPS, they showed completely different photocatalytic activities. This work demonstrated that the distribution of -OH groups over the surface of TiO_2 impose a significant influence on the photocatalytic ability and confirmed that doped photocatalysts with a low number of surface terminal hydroxyl groups had high photocatalytic activity. According to the results obtained from the high-field 1H MAS NMR, F-doped TiO_2 exhibited the maximum photocatalytic performance for the complete conversion of acetaldehyde because of the lowest number of the terminal hydroxyl group compared to the Cu-doped TiO_2. Acetonitrile is a highly volatile, poisonous, and stable chemical found in a variety of civic and industrial wastewater. Additionally, the indoor air is found to include acetonitrile, which is released by smoking tobacco, resins, and commercial fiber polymeric materials. Because it has both an alkyl as well as cyanide group that can go through various oxidation processes, acetonitrile serves as an intriguing model compound for photooxidation investigations [146]. Inturi and his team incorporated

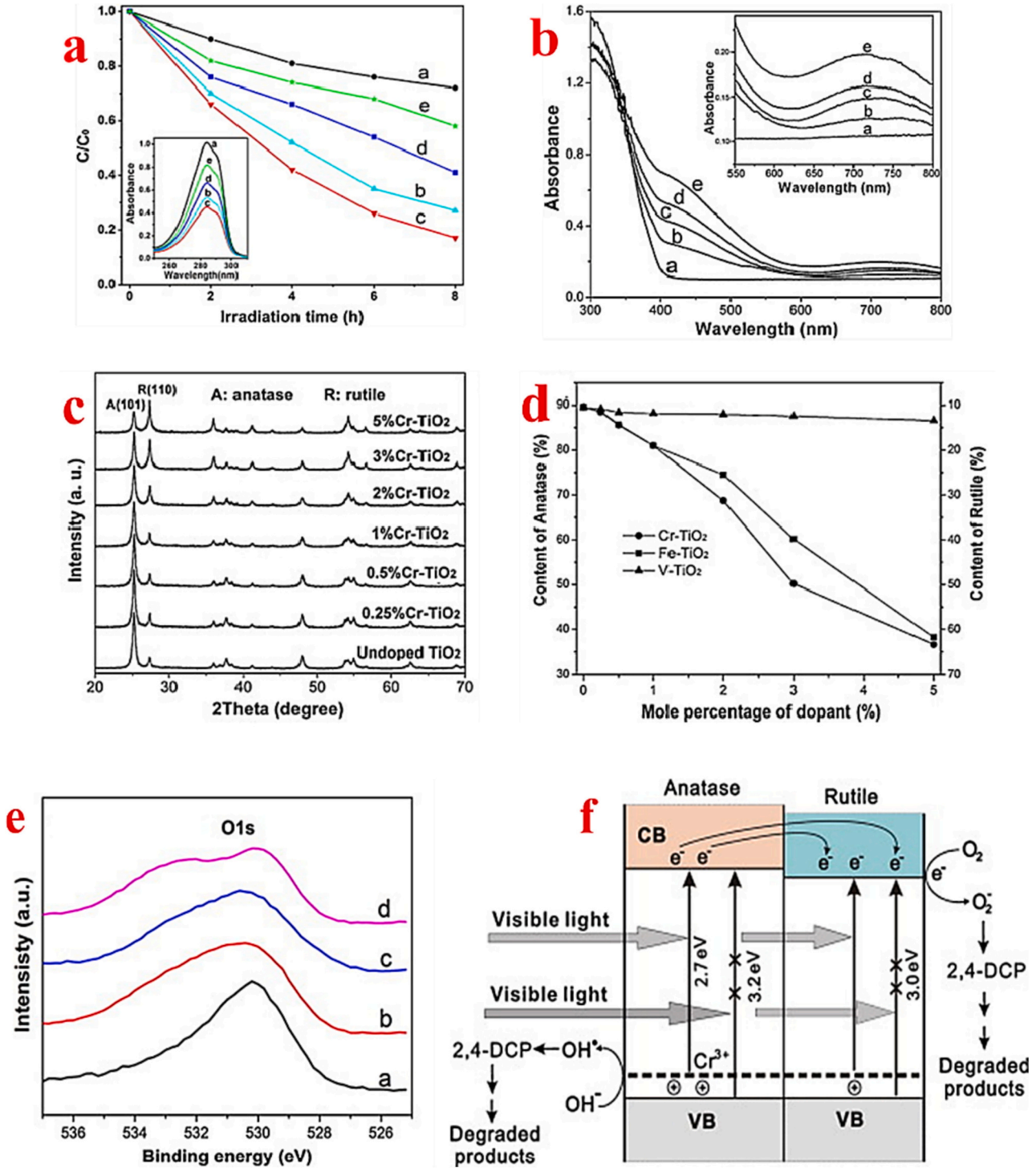

Fig. 10. Photo degradation of 2,4 DCP by various Cr-doped TiO_2 photocatalysts (a), UV- DRS spectra (b) of (a) undoped TiO_2, (b) 0.5% Cr-TiO_2, (c) 1% Cr-TiO_2, (d) 2% Cr-TiO_2, and (e) 5% Cr-TiO_2, XRD patterns of Cr-TiO_2 (c), content evolutions of anatase and rutile phases with doping concentration (d), core level spectra of O 1 s for undoped TiO_2, 1%, 2%, and 5% Cr-TiO_2, (e), and the photodegradation mechanism of 2,4 DCP over Cr-doped TiO_2 photocatalyst (f) [137].

various transition metals into TiO_2 using one-step liquid flame aerosol method [147]. The obtained photocatalysts were studied for the photodecomposition of acetonitrile in the gas phase. According to their temperature-programmed reduction studies, all the synthesized materials exhibited the formation of Me-O-Ti bonds. Titania and chromium have higher reducibility, hence the reduction peaks in chromium-doped titanium dioxide were pushed to much lower temperatures. The strong interactions and formation of Cr-O-Ti bonds in Cr/TiO_2 enable visible light absorption and facilitate efficient charge transfer processes. This is the main reson behind making it an active photocatalyst in the visible light range. However, the inactivity of the Mn^{3+}-incorporated TiO_2 catalyst was caused by the meager energy needed for electrons to escape from Mn^{2+}. Teoh and his colleagues employed one-step flame spray pyrolysis to synthesize Fe-doped TiO_2 using iron naphthenate and titanium isopropoxide as precursors for Fe and TiO_2, respectively for the photomineralization of oxalic acid under visible light irradiation [148]. They discovered a considerable enhancement in photocatalytic activity in comparison to the pure TiO_2, which is primarily attributed to special

Fe-leaching and re-adsorption capabilities. This investigation also proved excellent Fe-TiO_2 stability and repeatable mineralization rates even after five additional cycles. On the other hand, ferrocene possesses several properties that make it a favorable source of iron for iron-doping in titania nanoparticles including nontoxicity and solubility in liquid hydrocarbons [149]. In diffusion flames, silica nanoparticles and carbon nanotubes with controllable surfaces have been synthesized using ferrocene as a catalyst [150]. Carbon nanotubes (CNTs) [151], boron nitride/carbon nanotube composites (BN/CNTs) [152], metal oxides such as Al_2O_3 [153] and Fe_2O_3 [154], and thin films [155] were all produced using ferrocene in the flame spray pyrolysis process. In that sense, Ismail et al., employed a flame spray pyrolysis route to prepare Fe-doped TiO_2 using ferrocene and titanium tetraisopropoxide as sources of iron and TiO_2, respectively (Fig. 11a) [273]. The synthesized photocatalytic materials were tested for photoremoval of RhB under visible light illumination and observed the sample with 10% Fe/Ti demonstrated the highest catalytic activity (Fig. 11b&c). The uniform distribution of Fe across TiO_2, the diminished valence band edge (Fig. 11d), and the improved light absorption qualities (Fig. 11e) were the key causes of this high activity. Comparing these materials to undoped TiO_2, their better magnetic characteristics are in addition to their improved photocatalytic activity. Enhanced thermal stability of Pt/TiO_2 catalysts were obtained by Bi et al. [157] using in-situ N-doping and a second nozzle placed above the spray pyrolysis flame. The obtained materials were then examined for CO catalytic oxidation. The formation of Pt—N bonds on the catalyst's surface are responsible for the in-situ synthesis of surface N-doped Pt/TiO_2 and its superior thermal stability as compared to the pristine sample. Besides, the Pt particles experience less phase transition and less sintering during the calcination process. This study also showed that N alters the chemical environment

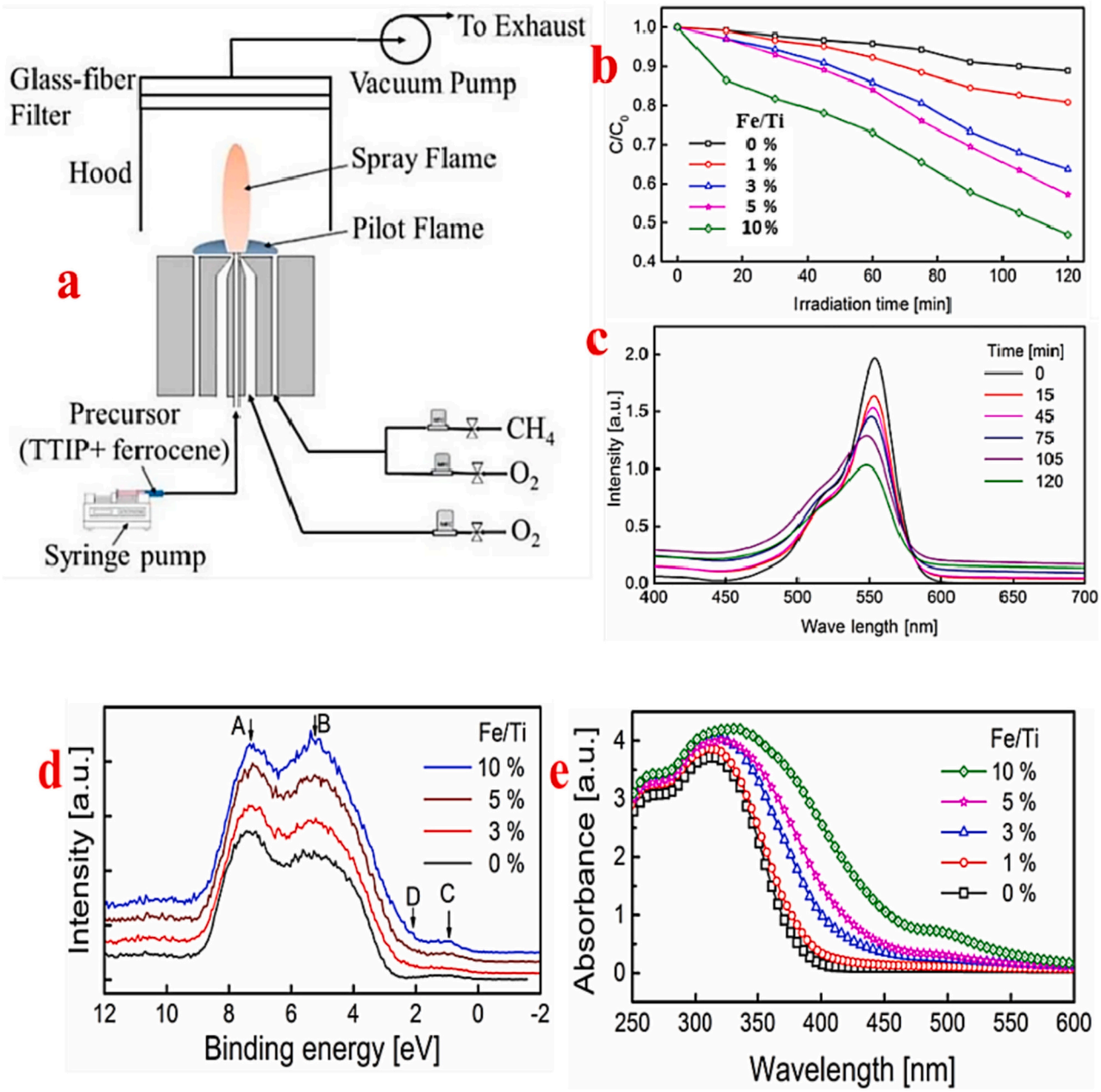

Fig. 11. Flame spray pyrolysis (FSP) approach (a), RhB degradation vs. irradiation time (b) and absorption spectra of RhB over Fe-TiO_2 (c), valence band for Fe-doped and pristine TiO_2 materials, suggesting for TiO_2 (A, B, and C) and for Fe (D) (d), and UV–Vis absorption spectra of pristine TiO_2 and various Fe-doped TiO_2 photocatalysts (e) [156].

around the Ti atoms and the ratio of surface oxygen species, which lowers the amount of adsorbed oxygen.

An efficient, low-temperature, and ecologically acceptable way to remove air pollutants is through photothermocatalytic oxidation. However, its widespread use has been severely constrained by the dearth of active, reasonably priced, and improved stability catalysts. The purification of gas streams containing toluene (C_7H_8), as a representative volatile organic molecule (VOCs) has drawn significant interest. It is well known that removing toluene has always been affordable thanks to low-temperature catalytic combustion [158]. However, higher temperatures are required in the thermal catalytic oxidation process, and the usual photocatalytic degradation mechanism has a poor degradation efficiency [159]. Thankfully, the photothermocatalytic combustion technique makes air pollution removal more effective at lower temperatures by fusing the advantages of thermal catalysis with photocatalysis processes [160]. Recently, Yuan and his coworkers studied the influence of single- Pt atom loading on TiO_2 support for enhancing the photothermocatalytic activity through flame spray pyrolysis towards toluene combustion [161]. Pt-loaded TiO_2 boosts the catalytic toluene removal for several reasons; first Pt cations are responsible for the TiO_2 phase transformation (anatase to rutile) and generation of surface oxygen vacancies. Second, is the introduction of defect energy levels that force the charge separation efficiency because of the presence of Pt 3d orbitals. Recently, composite oxide nanoparticles have received a lot of interest for enhancing the characteristics of single-component oxide nanoparticles. In tests for various photocatalytic applications, a variety of composite materials demonstrated improved photocatalytic performance compared to a single photocatalyst, mostly because of the increased efficiency for charge separation [162]. Cho et al. studied effect of the molar ratios of the constituents in TiO_2/SiO_2 composite onto the properties of synthesized particles by FSP method [163]. They investigated how spraying a mixture of tetra-ethylortho-silicate and titanium-tetra-isopropoxide led to the creation of mixed oxide nanoparticles of TiO_2 and SiO_2 with different compositions by flame spray pyrolysis technique. They also demonstrated that altering the molar ratio of the mixture affected the particle properties and optimized the photocatalytic activity of the TiO_2/SiO_2 composite towards the degradation of methylene blue. Cerium oxide (CeO_2) is a type of rare-earth oxide utilized in photosensitive materials, photoluminescence, and anti-UV radiations. This material has drawn substantial interest in catalysis owing to its capacity to function as an oxygen reservoir. This property arises from the redox shift between the Ce^{4+} and Ce^{3+} oxidation states under oxidizing and reducing conditions. It has already been documented that adding Ce atoms to TiO_2 increases photocatalytic activity [164]. Chaisuk and his team doped TiO_2 with CeO_2 by flame spray pyrolysis approach to fabricate a CeO_2-doped TiO_2 nanocrystalline photocatalyst [165]. Their study revealed that single-crystalline spherical particles consisting of CeO_2-doped TiO_2 nanopowders with particle sizes in the range 10–13 nm were generated at 5–50 at.% of Ce doping concentrations. Additionally, the absorption edge was moved to the visible area with Ce concentrations up to 30%. Tungsten trioxide (WO_3) is also considered a possible candidate to combine with TiO_2 to form a composite structure [166]. WO_3 is an effective photocatalyst due to the narrow energy band gap, making this semiconductor active in the visible light [167]. Arutanti et al. synthesized composite WO_3/TiO_2 nanoparticles by flame spray pyrolysis approach and employed ammonium metatungstate and titanium isopropoxide as precursors for the preparation of WO_3, and TiO_2, respectively [168]. Importantly, this study investigated the effect of the precursor's composition on the particle morphology, surface structure, and photocatalytic performance. It was observed that the amount of ammonium metatungstate (specifically 0 to 25 wt%) exhibited a great effect on the photocatalytic efficiency of the composite photocatalysts. The authors also postulated that the band gap energy and surface area are the main variables influencing variations in photocatalytic activity. Although Cr/TiO_2 has been recognized as an efficient photocatalyst for organic pollutant degradation, there is a concern regarding the potential leaching of chromium (Cr) from the catalyst into the fluid solution under visible light activity. Thus, the photocatalyst's capacity to be reused and stabilized may be hampered by the likelihood of Cr(VI) being reduced to Cr(III) [169]. In addition, some studies reported that the leaching of Cr in the fluid solution can cause secondary contamination [170]. For that, the use of supported TiO_2 could stabilize and enhance the photodegradation performance as compared to the pristine TiO_2 [171]. Silica (SiO_2) was the most used support for titania in photocatalysis due to several advantages such as improved electron absorption, higher adsorption, large surface area, and reduced UV light scattering [172]. Inturi et al. created a set of Ti/Cr/Si ternary composites using the FSP approach to stop Cr leaching and produce a highly visible light active photocatalyst [173]. Their findings demonstrated that the addition of Cr may modify the TiO_2 lattice's disorder, enhance crystallinity, and increase the catalyst's ability to absorb visible light. On the other hand, adding higher concentrations of Cr can decrease the photocatalytic activity due to the transformation from CrO_3 to Cr_2O_3 oxide. The incorporation of silica into TiO_2 can lead to enhanced photocatalytic performance by increasing the surface area and promoting the stability of the catalysts, thereby preventing the leaching of chromium (Cr) from the material. Among all prepared catalysts, the Cr/Ti/Si composites having Si/Ti atomic ratios = 75 and (Si + Ti)/Cr atomic ratios = 20 and 25 demonstrated an exceptional activity towards the visible-light-mediated degradation of phenol in aqueous solution. The same study team created identical photocatalysts using three distinct methods, such as sol-gel, coprecipitation, and flame spray pyrolysis, and assessed their efficacy in degrading 4-chlorophenol when exposed to visible light [174]. Of the three tested catalysts, the Cr/TiO_2 catalyst prepared by flame spray pyrolysis exhibited the highest activity (Fig. 12a) due to its high Cr^{6+} contents revealed by the temperature-programmed reduction profile (Fig. 12b). As presented in Fig. 12c, both sol-gel and coprecipitation method have only one oxidation state of Cr, on the other hand, the FSP Cr/TiO_2 presented two different peaks indicated two different oxidation states of Cr. In addition, silica was also used as a support for this photocatalyst to induce stability and reduced leaching of Cr from the material. The stability and hence leaching effect for the Cr into the liquid phase was examined under different pH solutions ranges from 3 to 11, and was discovered to be quite low compared to other synthesis techniques (Fig. 12c). In addition, compared to the other two ways, the Cr/TiO_2 produced by FSP had the largest surface area, significantly enhancing the photocatalytic efficacy (Fig. 12d). Finally, for the three synthesis methods, the Cr/TiO_2 photocatalyst demonstrated increased visible light absorption compared to pure TiO_2, which is mostly attributed to the excitation of the 3d electrons of Cr ion to the conduction band of TiO_2 as seen in Fig. 12e.

Similar Cr/TiO_2 photocatalysts were synthesized by the FSP method and tested for the oxidative conversion of acetonitrile in gaseous phase under visible illumination [175]. Photocatalyst having Ti/Cr atomic ratio equal to 40 displayed the highest activity which is mainly attributed to the existence of Cr^{6+} that strongly interacts with TiO_2. Besides the formation of strong interaction between the support and the dopant (Cr − O − Ti) revealed by H_2 − temperature programmed reduction (TPR) results are also one of the reasons responsible for the increased catalytic activity of the Cr/TiO_2 photocatalyst.

3.1.3. Photocatalytic CO_2 reduction (mechanism and activity)

Environmental pollution has recently gotten worse because of the atmosphere's rising CO_2 level, which is brought on by people and industry development using fossil fuels more and more [176]. As seen in Fig. 13a [177], the enormous consumption of fossil fuels over the past 35 years has caused a steady increase in annual CO_2 emissions [178].

The increase in CO_2 emissions over the past 35 years has been accompanied by a rise in the average world surface temperature, which is not surprising considering the potential of CO_2 accumulation to trap heat in the atmosphere. Finding ecologically friendly and renewable energy sources is now of utmost importance to improve human

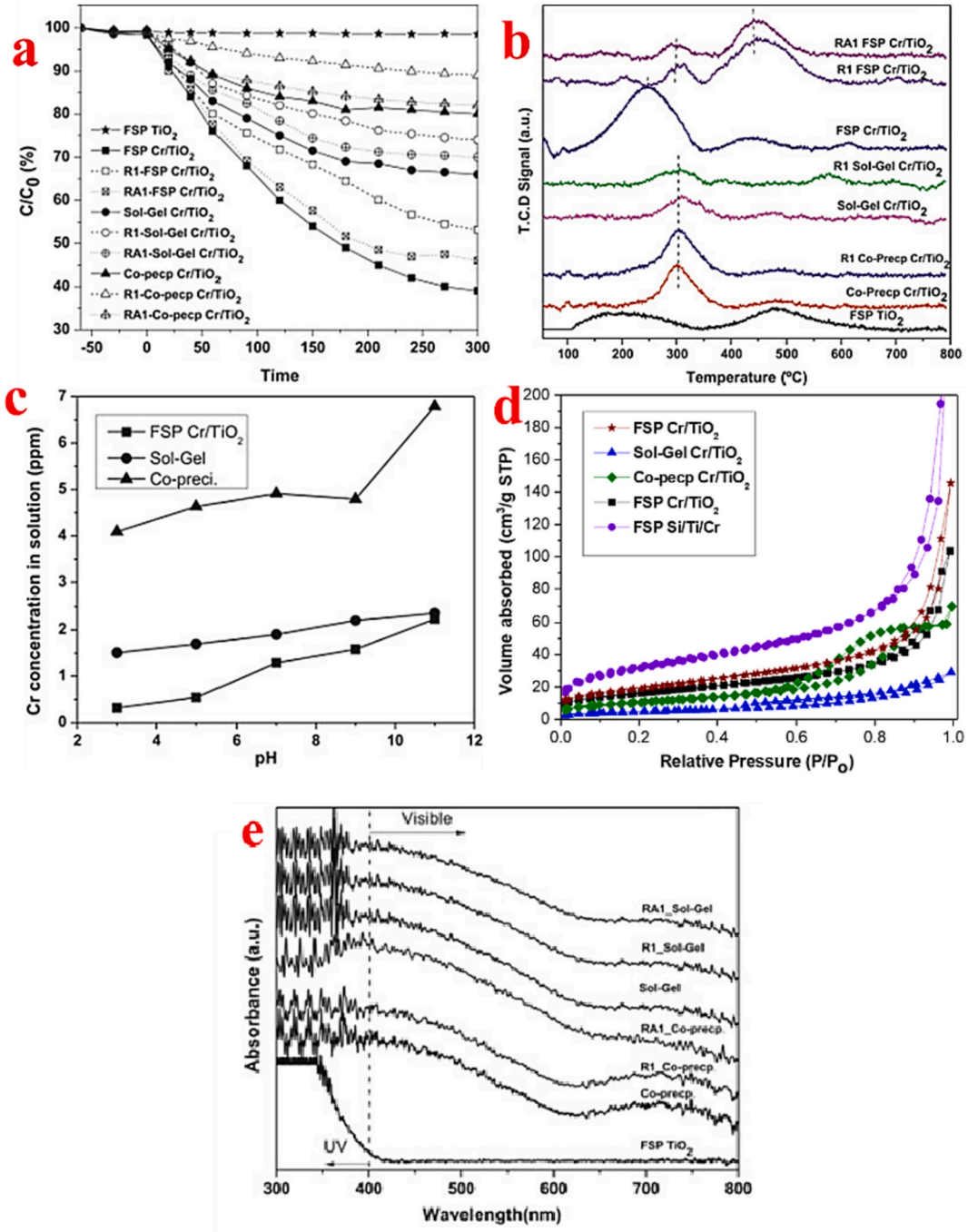

Fig. 12. Visible light photocatalytic conversion of 4-chlorophenol by Cr-TiO_2 photocatalyst prepared by three methods with reused and reactivated catalyst (a), H_2-TPR profiles of fresh, reactivated catalysts prepared by FSP TiO_2, FSP Cr/TiO_2, sol-gel and co-precipitation (b), Effect of medium pH on leaching of Cr in Cr/TiO_2 (c), N_2 adsorption-desorption isotherms of Cr/TiO_2 catalysts (d), and UV–vis DRS of fresh, reactivated catalysts prepared by the three methods (sol-gel, coprecipitation, and FSP) (e) [174]. The revived catalyst was designated with the prefix RA, and the number of re-activation cycles was shown after. R stood for materials that are reused without activation.

civilization over the long run [179]. Thus, the conversion of solar energy into valuable solar fuels has received a lot of interest because it is thought of as one of the unlimited and environmentally friendly energy sources [180]. Hence, the production of green solar fuels including methane (CH_4), formic acid (HCO_2H), formaldehyde (CH_2O), and methanol (CH_3OH) through photocatalytic CO_2 reduction has been hailed as one of the most promising technologies among different options since it can replicate atmospheric CO_2 levels while also producing valuable solar fuels [181]. Since the first publication by Inoue et al. in 1979 [182], several semiconductors have been developed as photocatalysts for efficient CO_2 reduction, including TiO_2 [183], CdS [184], Fe_2O_3 [185], g-C_3N_4 [186], Bi_2WO_6 [187], and Cu_2O [188]. Among these photocatalytic semiconductors, TiO_2 has drawn a lot of interest as a highly promising photocatalyst for the reduction of CO_2.

Photocatalytic reduction of CO_2 mimics the natural photosynthesis process, by turning incoming solar radiation to produce useful solar fuels without the requirement for extra high-energy input [189]. Because of this, it has become the technique for producing oxygenated hydrocarbons that has been most intensively studied. Photocatalytic CO_2 reduction process is often divided into four major phases (see

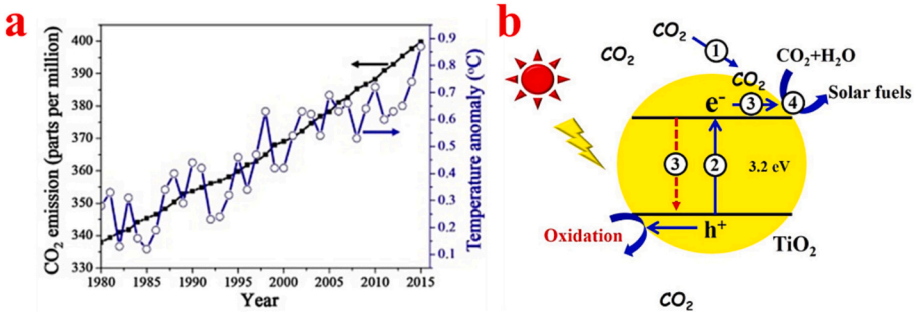

Fig. 13. The variations between in annual CO_2 emissions and the average global surface temperature between 1980 and 2015 (a) [177], and the four steps for photocatalytic CO_2 reduction (b) [190].

Fig. 13b) [190]. (1) CO_2 adsorption which is the rate-limiting step for the overall process, (2) light absorption and electron-hole pairs generation, (3) charge separation and immigration, and (4) CO_2 reduction [191]. The capacity of TiO_2 to adsorb CO_2 molecules is a crucial factor that impacts the photocatalytic CO_2 reduction performance of this material. Surface modification in TiO_2 can enhance its specific surface area and the number of surface active sites, which will improve its ability to bind CO_2 [192]. Additionally, modifying the TiO_2 surface to have an alkaline characteristics is another practical technique to increase its capacity for CO_2 adsorption by CO_2 chemisorption [193]. Additionally, a crucial method to improve the photocatalytic activity of TiO_2 towards CO_2 reduction is to decrease its bandgap by doping [194]. In addition to doping, surface loading by the metal plasmonic nanoparticles can be utilized to boost up the photocatalytic activity by infusing "hot electrons" into TiO_2 to enhance the efficiency of the generation of electron-hole pairs [195]. Another method to drive TiO_2's photocatalytic CO_2 reduction by reducing charge recombination rates is to add a cocatalyst to its surface [196]. Finally, CO_2 reduction can be accomplished by using the charge carriers (e^- and h^+ pairs) that are moving towards the TiO_2 surface. But keep in mind the extraordinary stability of the CO_2 molecules. [197]. Thus, the e^- possessing a high enough reduction potential only, can be used in specific CO_2 reduction reactions as illustrated in the CO_2 reduction equations including standard redox potentials reviewed by Low et al. [190]. Only CH_4 and CH_3OH can be produced by TiO_2 during a photocatalytic CO_2 reduction reaction because the conduction band potential of TiO_2 is −0.5 V vs. NHE at pH = 7 [198]. It should be noted that the creation of CH_3OH (6 e^-) and CH_4 (8 e^-) also requires multielectron reactions [199]. As a result, accumulating electrons on specific TiO_2 reaction sites is highly sought to achieve multielectron transfer.

It has been claimed that modifying TiO_2 with transition metals like Cu [200], or noble metals like Pt [201], or Ag [202] is a successful way to increase CO_2 photocatalytic reduction. This is because the metal atoms can boost separation of charge carriers, and increase light absorption, or CO_2/H_2O chemical adsorption. Among the various material in the series, Cu-modified TiO_2 has garnered the most interest of these because of the high performance and affordable price of Cu [203]. According to some reports, Cu in the Cu/TiO_2 photocatalyst may exist in a variety of forms and chemical states, including Cu^0, Cu^+, and Cu^{2+} (e.g., oxide deposited on a TiO_2 surface or ions doped inside the TiO_2 lattice) [204]. It offers a potential method to modify the characteristics of the Cu/TiO_2 photocatalyst. However, it also introduces challenges to comprehend the specific functions of the Cu species within the catalyst. The coexistence of different Cu species with different oxidation states and/or forms and coupled with the potential for exchange between them during the CO_2 photoreduction reaction complicates the analysis of their individual roles [205]. In that sense, Xiong, and his team incorporated Cu^+ into the TiO_2 lattice using a FSP synthesis route using copper nitrate and titanium butoxide as precursors for Cu and TiO_2, respectively and demonstrated outstanding activity and stability in photocatalytic reduction of CO_2 [206]. The CuTi-1 catalyst exhibited the highest yields of CO and CH_4, reaching 43.5 and 16.7 μmol g^{-1} after 4 h of light irradiation (Fig. 14a&b). Additionally, this photocatalyst showed good stability under 4 h irradiation (Fig. 14c). This high activity was mainly attributed to the high distribution of Cu species and existed as a dopant rather than as oxides like Cu_2O or CuO crystals deposited on the surface as shown in the HRTEM (Fig. 14d). Furthermore, the enhanced photocatalytic activity was also ascribed to the enhanced visible light absorption, and improved charge separation efficiency in the CuTi-1 sample as proved by the UV–Vis absorption and photoluminescence spectrums (Fig. 15a-c). The existence of Cu(I) was revealed using the XPS spectra and showed that the peak located at approximately 932.5 eV corresponds to the Cu $2p_{3/2}$ levels in the case of high activity photocatalyst (CuTi-1) demonstrating that the Cu existed as Cu(I) in the material CuTi-1 (Fig. 14d).

3.1.4. *Photocatalytic removal of NOx*

It has been established that NOx (NO + NO_2) may be a factor in respiratory illnesses and acid rain [207]. Photochemical oxidation (PCO), which uses photocatalysts, has been developed in a variety of systems to remove NOx from the environment. As mentioned before, TiO_2's limited capacity to absorb visible light is a result of its large bandgap. Recently, most research has focused on cocatalysts that contain transition metals, noble metals, or non-metal elements to reduce their band gap energies that make them able to absorb under visible light illumination (Table 3). For example, noble metal co-catalysts can enhance the activity of this catalyst by lowering TiO_2's effective bandgap, supplying additional active sites, and generating localized surface plasmon resonances. Fujiwara and his team produced Pd/TiO_2 particles by flame spray pyrolysis for NOx removal under solar light irradiation [208]. There is a linear relationship between percentage of isolated Pd atoms and the total Pd content. Originally isolated Pd atoms rose linearly with rise in the total Pd content, as measured by diffuse reflectance infrared Fourier transform spectroscopy. It eventually reaches a equilibrium value of 0.055% of the total Pd content when the total Pd content reaches 0.1 wt%. Due to the development of Pd clusters, further rise in the Pd concentration do not significantly result in more isolated Pd atoms. Despite of the limited presence of isolated Pd atoms, their impact on photocatalytic activity was significant. This work showed that 0.1 wt% and 1 wt% doping in the $Pd\text{-}TiO_2$ co-catalyst lead to a linear improvement in the average NO removal capacity, corresponding to the proportion of isolated Pd atoms. Similar catalytic efficiency for Pd suggests that Pd nanoparticles, clusters, and distributed in bulk TiO_2 only play a modest role in the catalytic process. The remarkable activity of single Pd atoms in the photocatalytic removal of NO demonstrates their ability to provide extraordinarily active sites. These isolated Pd atoms exhibit exceptional selectivity for converting NO to nitrate, and they also display remarkable resistance to nitrate poisoning. Other single-atom catalysts (SACs) and corresponding applications in photo-electrocatalysis in the decontamination of various

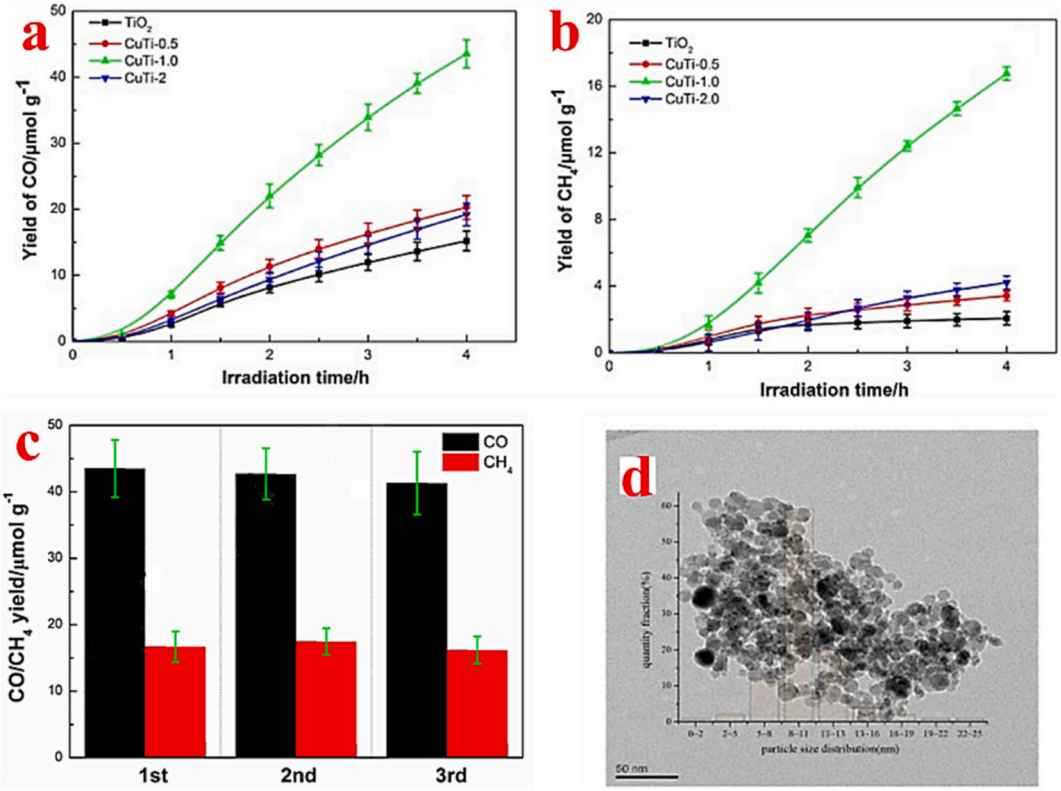

Fig. 14. CO (a) and CH_4 yields (b) over various Cu-modified TiO_2 synthesized by the FSP, three cycles stability test for CO and CH_4 production over CuTi-1 photocatalyst (c), and the HRTEM for CuTi-1(d) [206].

organic pollutants such Fe single-atom catalysts (Fe-SACs), Mn single-atom catalysts (Mn-SACs) were also reported [209,210]. Additionally, Metal-organic frameworks (MOFs) have gained significant attraction primarily because of their unique porous structure, and open metal sites and showed outstanding activity in the degradation of various organic pollutants in wastewater [211]. Graphitic carbon nitride (g-C_3N_4) has emerged as a widely adopted and innovative metal-free photocatalyst with good activity, and high chemical and thermal stability, making this photocatalyst a suitable candidate for different photo-catalytic applications [212,213]. Nevertheless, its high charge recombination rate reduces its large scale application. According to prior research, securing aromatic rings to the surfaces of CN might enhance charge pair separation, and thereafter improve its photocatalytic activity for removing sulfamethazine (SMZ) [214]. Further recent examples of applications of TiO_2-based photocatalysts were also summarized in Table 3.

3.2. *Thermocatalysis*

3.2.1. *CO_2 methanation*

As per the provisions of 2015 Paris Climate Agreement, the goal is to limit the rise in global temperatures to a maximum increase of 1.5 to 2 °C [215]. After that, a number of techniques have been put forth to reduce CO_2 emissions caused by extensive use of fossil fuels including carbon capture and utilization. An appealing and effective solution to the issues is to convert CO_2 into value-added fuels in a sustainable manner [216]. CO_2 methanation i.e. conversion of CO_2 into methane ($CO_2 + 4H_2 \rightarrow CH_4 + 2H_2O$) as one of the several CO_2 hydrogenation processes, is gaining interest owing to the high combustion value of CH_4 and its capability to be used directly in the present natural gas infrastructure. Nevertheless, intrinsic inertness of CO_2 prevents the application of this strategy, though. It is crucial to do this by creating catalysts with strong selectivity for CH_4 at lower temperatures of <400 °C. Different transition metals have so far been thoroughly investigated for CO_2 methanation, including Rh, Ru, Ni, and Co [217]. Ru and Rh have outstanding catalytic characteristics, but their exorbitant cost prevents their widespread applications. TiO_2 is considered one of the most efficient photo-or thermocatalytic catalysts for CO_2 reduction. Recently, Yang et al. employed theoretical investigations and surface reaction chemistry to describe the reaction mechanism of CO_2 methanation over Rh/TiO_2 catalyst (Fig. 16) [218]. In comparison to the formate and direct C—O bond cleavage pathways, the Rh/TiO_2 catalyst is substantially less thermodynamically and kinetically favorable for CO_2 methanation than the reverse water–gas shift (RWGS) reaction followed by CO hydrogenation (Fig. 16). They concluded that the metal-support interface's periphery is a major area of charge buildup that can supply electrons needed for CO_2 reduction to make CH_4. Activation of CO_2 is more feasible at the interface active site than at the Rh nanoparticle location. The most active site of CO_2 adsorption and activation over Rh/TiO_2 catalyst is the metal-support contact. Modified TiO_2 holds significant promise as a photo- or thermocatalytic catalyst, making it a valuable candidate for CO_2 thermal methanation. For example, Kolb et al. [219] found outstanding methanation efficiency on Ru/TiO_2 {001} due to the positive MSI effect. Recent applications of TiO_2 catalyst for thermal methanation are summarized in Table 3.

3.2.2. *Volatile organic compounds (VOCs)*

One type of typical volatile organic compound (VOCs) is toluene. Both the environment and human health are seriously harmed by its neurological toxicity and precursor for photochemical haze. Toluene concentrations of hundreds ppm can cause severe pain, and prolonged exposure can have fatal consequences [219]. Such a pollutant may be created from several types of sources, like industrial emissions, biomass usage, painting, and vehicle exhaust. Much consideration and recognition are given to the catalytic oxidation of toluene at low temperature, as a potentially effective method for eradicating industrial pollution on a broad scale. Although noble metals showed outstanding thermal

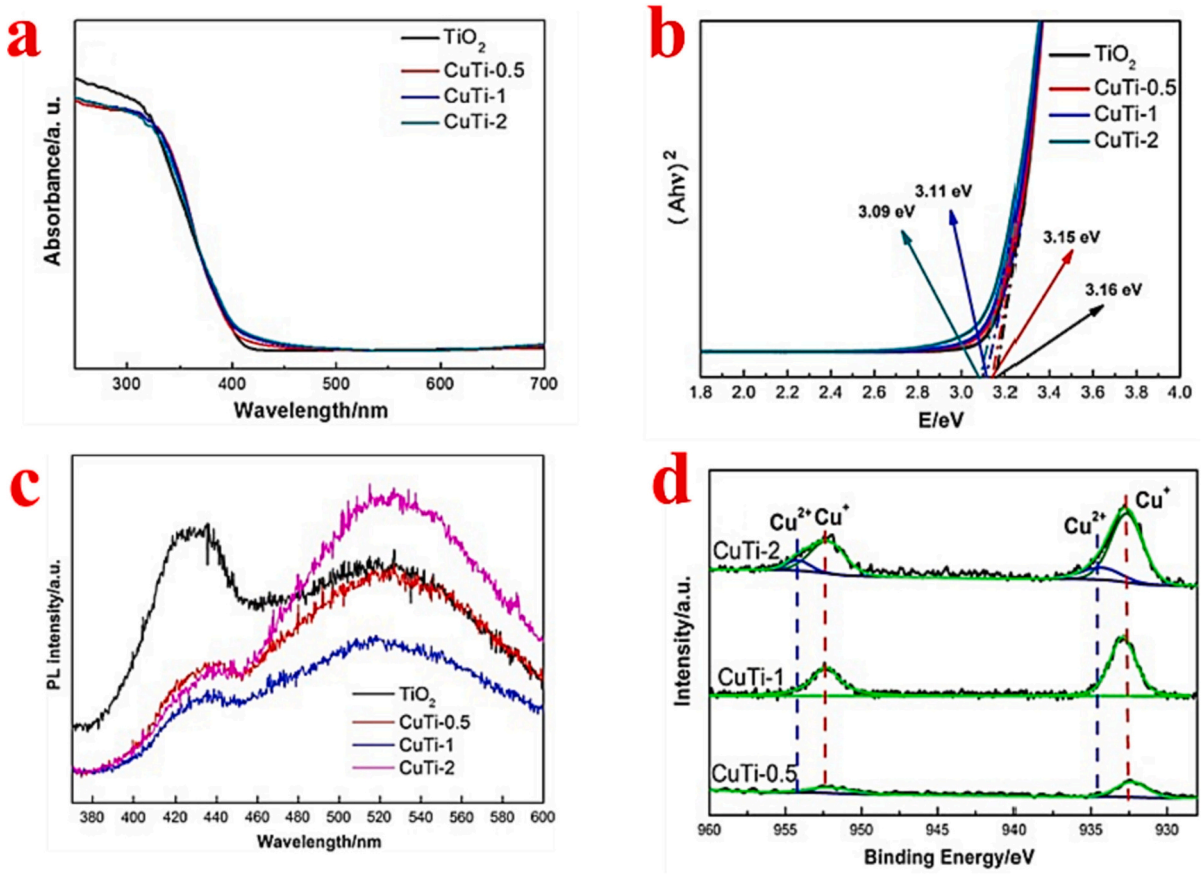

Fig. 15. UV–vis DRS absorption spectra (a), Tauc plots (b), and photoluminescence (c), and the Cu2p XPS spectra of different Cu-modified TiO_2 photocatalysts (d) [206].

catalytic activity on toluene removal at low temperatures, their high cost and scarcity reduced their large-scale utilization. Thus metals/transition metals can be brilliant alternatives to precious metals because of their less price, higher durability, and capable performance. Among these, TiO_2 showed acceptable thermal catalytic activity for VOCs removal due to its excellent oxygen storage ability as well as large specific surface area. Meng et al., synthesized highly active CuO-TiO_2 nano-catalysts using FSP for toluene removal at 250 °C [220]. The stable existence of highly distributed CuO, low-temperature reducibility, and large specific surface area are primarily accountable for the catalyst's high activity. Further recent examples of the applications of TiO_2-based catalysts for VOCs removal are summarized in Table 3.

3.3. Electrocatalysis

Electrocatalysts are crucial components in energy conversion and storage systems like fuel cells [221] and water-splitting devices [222]. However, their use has frequently been constrained by poor manufacturing rates and high fabrication costs. Flame spray processing enables the scalable manufacture of electrocatalysts and makes it simple to customize the electronic structure by adjusting the processing settings. We thus think that this area has a lot of potential for both fundamental research and real-world practical applications, despite the fact that only a limited number of publications have documented the flame aerosol synthesis of electrocatalysts thus far.

3.4. Organic transformation

3.4.1. Hydrogenation of 3-nitrostyrene

Functionalized anilines play a vital role as essential industrial intermediates in the production of various compounds, including pharmaceuticals, polymers, herbicides, and fine chemicals. Specifically, chemoselective hydrogenation of nitrostyrene into vinylaniline over Pt/TiO_2 catalyst is illustrated in Fig. 17 [233] is a key reaction for creating the intermediates needed to make pharmaceuticals, dyes, and pigments.

However, since these molecules have two functional groups, one is a carbon-carbon double bond (C═C) and another one being —NO_2 group, it becomes very challenging to selectively reduce the nitro group specifically, when many reducible groups are present within the same entity. In earlier investigations, for instance, cobalt and ruthenium sulfide catalysts were utilized to selectively hydrogenate nitro compounds into amines when olefinic groups were present [234]. However, the low yields and the formation of by-products that contain sulfur severely restrict the applicability of these materials. Other catalyst systems with practical limitations in terms of reuse included iron complexes [235] and doped Raney nickel [236]. Carbonyl and double bonds can all be activated by noble metal catalysts, as well as nitro groups, resulting in an unselective reduction [237]. Flame spray pyrolysis has been extensively explored and used in a variety of reactions, including lean-NOx storage reduction, methane catalytic combustion, hydrogenation, dehydrogenation, and photocatalysis [238]. For example, Pt/Al_2O_3, Pd/Al_2O_3, and Pd/SiO_2 composite catalysts produced by FSP exhibited greater catalytic efficiencies in hydrogenation as compared to the reference catalysts generated using the traditional impregnation approach [239]. Pt-based catalysts are frequently utilized in the hydrogenation of nitrostyrene due to their high catalytic efficiency; nevertheless, the catalytic material also concurrently hydrogenates both the functional groups, resulting in an unselective reduction. This problem may be solved in a variety of ways, such as by using modifiers, changing the pretreatment conditions, and offering catalytic support [240]. Cobalt serves as an intriguing catalyst

Table 3
Thermal, photo, and electrocatalysts synthesized by FSP in the last 5 years.

Material	Method	Chemical reaction	Optimal efficiency	Year	Reference
Pt/TiO_2	FSP	CO oxidation	T100 ≈ 120 °C, T50 ≈ 110 °C; CO reaction rate 0.13×10^{-7} mol s^{-1} $gcat^{-1}$	2018	[223]
Pt/TiO_2	FSP	Methane consumption	85% methane conversion (600 °C)	2018	[224]
$Au\text{-}Pd/TiO_2$	DFSP	Acetylene hydrogenation	96% C_2H_4 selectivity (40 °C) 45% C_2H_2 conversion	2018	[225]
Ag/TiO_2	FSP	Nitrate reduction	14.5% NO^{3-} conversion under 200 W Hg light	2019	[226]
$N\text{-}/TiO_2$	FSP	Phenol degradation	50% phenol degradation	2018	[227]
Other catalysts					
$PrBaCo_2(_{1x})Fe_{2x}O_{6\text{-}\delta}$	FSP	Oxygen evolution reaction	19.7 A g^{-1} current density at 1.55 Vs. RHE	2019	[228]
$Ru/SiO_2\text{-}Al_2O_3$	FSP	Fischer-Tropsch synthesis	37% CO conversion at 240 °C	2020	[229]
$Ni\text{-}Co/Al_2O_3\text{-}La_2O_3$	FSP	Methane dry reforming	80% methane conversion	2018	[230]
Cu/ZrO_2	FSP	CO_2 hydrogenation into methanol	2–4% CO_2 conversion.	2020	[231]
$SiO_2\text{-}Al_2O_3$	FSP	Transformation of glucose to levulinic acid	100% glucose conversion at 180 °C	2020	[232]

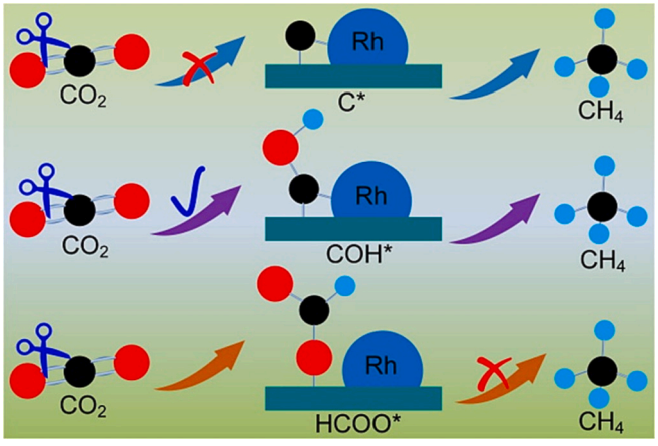

Fig. 16. Proposed mechanisms of CO_2 methanation [218].

particularly in hydrogenation reactions. It acts as a promoter for Pt-based catalysts by exerting both electrical and geometric effects [241]. Thus, when Co was added to Pt-based catalysts, catalytic performances were enhanced in comparison to Pt monometallic catalysts [242]. Pisduangdaw and his team used the flame pyrolysis via one-step approach for the selective hydrogenation of 3-nitrostyrene [243], they loaded Pt/

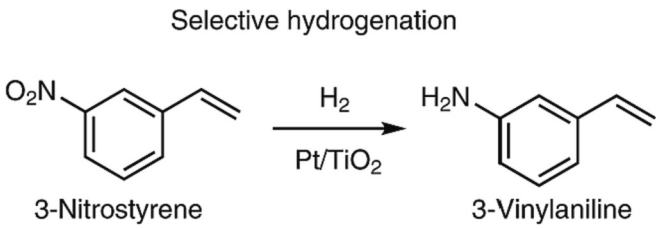

Fig. 17. Selective hydrogenation of nitrostyrene into vinylaniline over Pt/TiO_2 catalyst [233].

TiO_2 catalysts with different weight ratios of Co. Infrared spectroscopic measurements of adsorbed CO show that the incorporation of Co enhanced the amount of platinum terrace atoms on the catalyst surface, and increased the selective formation of ethylnitrobenzene. It was found that addition of cobalt to Pt/TiO_2 led to a significant enhancement in the hydrogenation activity and selectivity of vinylaniline and outperformed those of monometallic compound. These improvements were attributed to the strong forces of interactions between Pt—Co and the transfer of TiO_x species. The same research group also reported the influence of preparation methods (impregnation and flame spray pyrolysis) and reaction temperatures on the physicochemical as well as the catalytic properties of Pt/TiO_2 catalysts [244]. The F-Pt/Ti catalysts (F: catalyst prepared using flame spray pyrolysis route) exhibited higher dispersion of Pt (Fig. 18a&b) and better catalytic performance in liquid-phase hydrogenation reaction of 3-nitrostyrene (Fig. 18c). Among all the synthesized materials, F-Pt/Ti-600 showed the highest activity and selectivity. Furthermore, the H_2-TPR data showed that the F-Pt/Ti catalyst had lower Pt/Pt-TiO_x H_2 consumption ratios and demonstrated greater metal-support interaction as compared to the I-Pt/Ti catalyst (I: catalyst prepared using impregnation method) (Fig. 16 8d).

3.4.2. *Hydrogenation of 1-heptyne*

Industry, academia, and synthetic organic chemistry all benefit from the partial hydrogenation reaction of unsaturated organic molecules. This process is particularly important for the preparation of fine organic compounds, such as the selective hydrogenation of alkynes to their corresponding alkenes. The alkene compounds generated by this process are useful for the creation of biologically active chemicals, margarine, lubricants, and fundamental intermediates for the fine chemicals including food, pharmaceuticals, and cosmetics [245]. Catalytic hydrogenation is commonly performed in a liquid phase using batch-type slurry procedures, employing a supported noble metal catalyst due to the relatively mild reaction conditions that are needed and the simplicity of the catalyst separation [246]. Alkyne to alkene semi-hydrogenation is a common process carried out in both industrial settings and academic research labs using Pd-based catalysts because of their well-known high selectivity. Pd catalysts have been supported by a variety of materials in the selective hydrogenation process of alkyne, involving silica [247], alumina [248], carbon [249], and titania [250]. The Pd catalysts' activity, selectivity, recycling, and repeatability can all be greatly enhanced by selecting effective support. Titania (TiO_2) is an interesting support material for Pd catalysts in hydrogenation reactions. This is due to its strong metal-support interaction (SMSI) effect that makes it particularly important for Pd catalysts. It has been found that noble metals supported on reducible oxides, such as titania, demonstrate variations in catalytic activity and selectivity when subjected to high-temperature reductions. Additionally to supported monometallic nanoparticles, supported bimetallic nanoparticles are crucial for several catalytic reactions. Important examples include Au—Pd catalysts, which are employed in procedures like the selective conversion of alkenes to epoxides, alcohols to ketones or aldehydes, and hydrogen to hydrogen peroxide [251–256]. The synergistic effects caused by both ligand effects and ensemble effects of the Au—Pd alloy have frequently been cited as the cause of the Au promotional effects in Au—Pd catalysts.

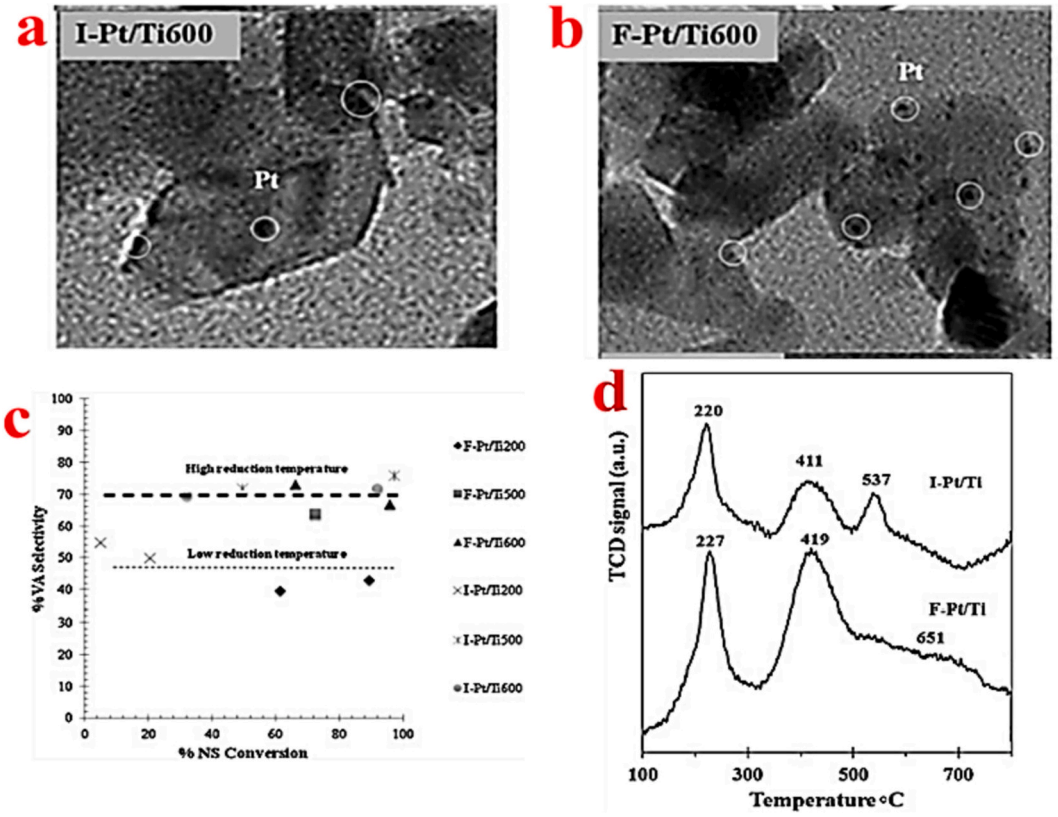

Fig. 18. TEM images of I-Pt/Ti (a), F-Pt/Ti (b) effect of reduction temperatures for the catalysts with the performance graph between nitrostyrene conversion and vinylaniline selectivity (c), and H_2-TPR profiles of Pt/TiO_2 obtained by impregnation (I) and flame spray pyrolysis methods (F) [244].

Numerous investigations have shown that the modulation of the selectivity and catalytic activity in hydrogenation processes is attributed to the electron transfer occurring between Pd and Au species [257]. However, it appears that a few parameters, including the molar ratio of the constituents, the manufacturing procedure, shape or size of the particles in Au—Pd alloys, affect the electrical interactions between Au and Pd species [258]. Bimetallic Au-Pd/TiO_2 nanoparticles has successfully been produced using single-step FSP, which does not require post-treatment processes like filtering, washing, drying, or calcination [259]. Pongthawornsakun and his colleagues used flame spray pyrolysis to create $AuPd/TiO_2$ bimetallic catalysts. They then reduced the catalysts for two hours at 40 and 500 °C. The synthesized materials were then investigated for the selective hydrogenation of 1-heptyne in liquid phase under moderate conditions [260]. The highest yield and selectivity towards 1-heptene was exhibited by the material $AuPd/TiO_2$ when reduced at 40 °C (20 min) (Fig. 19a&b). On the other hand, reduction at 500 °C manages to homogenize the individual Au—Pd nanoparticles and no substantial changes in bulk composition and the average crystallite sizes were observed. Moreover, a comparable level of strong-metal support interaction effect was observed in the case of bimetallic $AuPd/TiO_2$ during reduction at 500 °C same as exhibited by the monometallic one. In the end, the authors concluded that reduction at high temperatures is unwarranted for the advancement of catalyst performances when employing supported bimetallic AuPd catalysts.

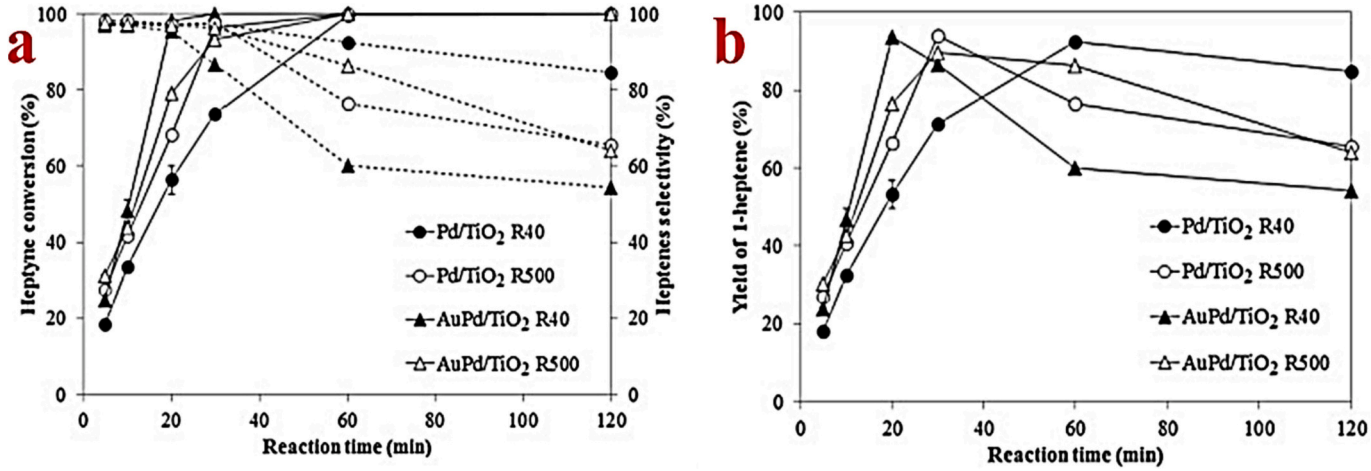

Fig. 19. Conversion and selectivity of heptyne to 1-heptene (solid line & dash line respectively) (a), and yield of 1-heptene (b) [260].

3.4.3. Hydrogenation of furfural

The increasing need for energy and chemicals on a global scale, as well as concerns over the impacts on the environment and the depletion of petroleum reserves, have all led to a great deal of interest in non-fossil carbon resources as an alternative sustainable resource. Lignocellulose biomass is the most accessible, commercially feasible, and promising resource for a sustainable alternative feedstock for making biofuel and biochemicals. In particular, the development of biochemicals, as opposed to petroleum obtained from fine chemicals, is a more intriguing alternative than the creation of biofuel, to boost the economic value. The chemical molecule furfural, which is generated from hemicellulose biomass, is one of the crucial intermediary platforms for many different components and chemicals for biofuels. Catalytic hydrogenation of furfural is an important process since it yields substances like tetrahydrofurfuryl alcohol, furfuryl alcohol, cyclopentanone, and 2-methylfuran [261]. According to reports, 62% of the furfural produced is utilized to create furfuryl alcohol (FA) [262]. Lysine, vitamin C, fine chemicals, agrochemicals, perfumes, lubricants, dispersion agents, plasticizers, and the synthesis of fibers are all produced using furfuryl alcohol. Liquid resins for reinforcing ceramics are another application for furfuryl alcohol [263]. FA is created by selectively hydrogenating the alcohol O—H group to the aldehyde C═O functional group. In the industrial setting, either the vapor or liquid phase could be used to perform the selective conversion of furfural to FA [264]. The most popular approach for industrial FA synthesis has been carried out for decades using copper chromite taken as the catalysts and reaction carried out at high temperature and pressure [265], which is also shown moderate activity [266]. In addition, the toxicity of chromium oxides is widely regarded as the greatest drawback of environmental pollutants [267]. As a result, there is rising interest in creating Cr-free FA synthesis catalysts that have high activity and selectivity as well as being environmentally responsible. Platinum-based catalysts have been identified as promising alternatives to traditional copper chromite catalysts for the hydrogenation of furfural. This is because platinum-based catalysts exhibit the ability to effectively reduce the carbonyl C═O group in furfural during hydrogenation processes [268]. Recently, Tolek et al. synthesized Pt/TiO_2 and $PtCo/TiO_2$ catalysts via FSP route and tested for hydrogenation of furfural to furfural alcohol (50 °C and 2 MPa H_2) as shown in the Fig. 20a [269]. Compared to the conventional impregnation method, anatase phase in TiO_2 dominated, and FSP showed the acceleration of rutile phase formation (Fig. 20b). According to the H_2-TPR analysis (Fig. 20c), the (F: flame spray pyrolysis)) Pt/TiO_2 catalyst's reduction peak of the Pt-TiO_x interface sites changed towards a higher temperature and grew wider than that of the (I: impregnation methods). Pt/TiO_2 indicated a stronger metal-support interaction effect brought about by the FSP approach. However, it is possible to infer that adding Co to the FSP-made catalyst was not required to improve the interaction of the metals with the support to increase the selectivity towards furfuryl alcohol.

3.4.4. Catalytic oxidation of CO

Carbon monoxide (CO) is a prominent and hazardous gas that exist in the environment and extensive efforts have been made to effectively eliminate it from the air. Incomplete oxidation of molecules containing carbon results in the formation of CO in the atmosphere. A small amount of CO can cause hypoxia, neurological and brain damage [270]. CO affects both people and other living things through its interference with plant respiration system and nitrogen fixation process. CO is an important active trace gase found within the earth's crust, and it has a substantial effect on both the atmosphere's and the environment's chemistry [271]. The major sources of the enormous CO emissions into the atmosphere are transportation, power plants, industry, and human habitation. The catalytic oxidation of CO plays a vital role due to its extensive utilization across various domains. It finds wide applications in household settings, exhaust air purification technologies for vehicles, CO gas sensors, and the functioning of CO_2 lasers [272]. Noble metals like Au [273], Pt [274], and Pd [275], as well as transition metals like Cu [276], are used as catalysts in the CO oxidation catalytic systems. The possible catalytic cycle for CO oxidation on Au/TiO_2 is shown in Fig. 21 [273].

Although supported Au catalysts have recently received much

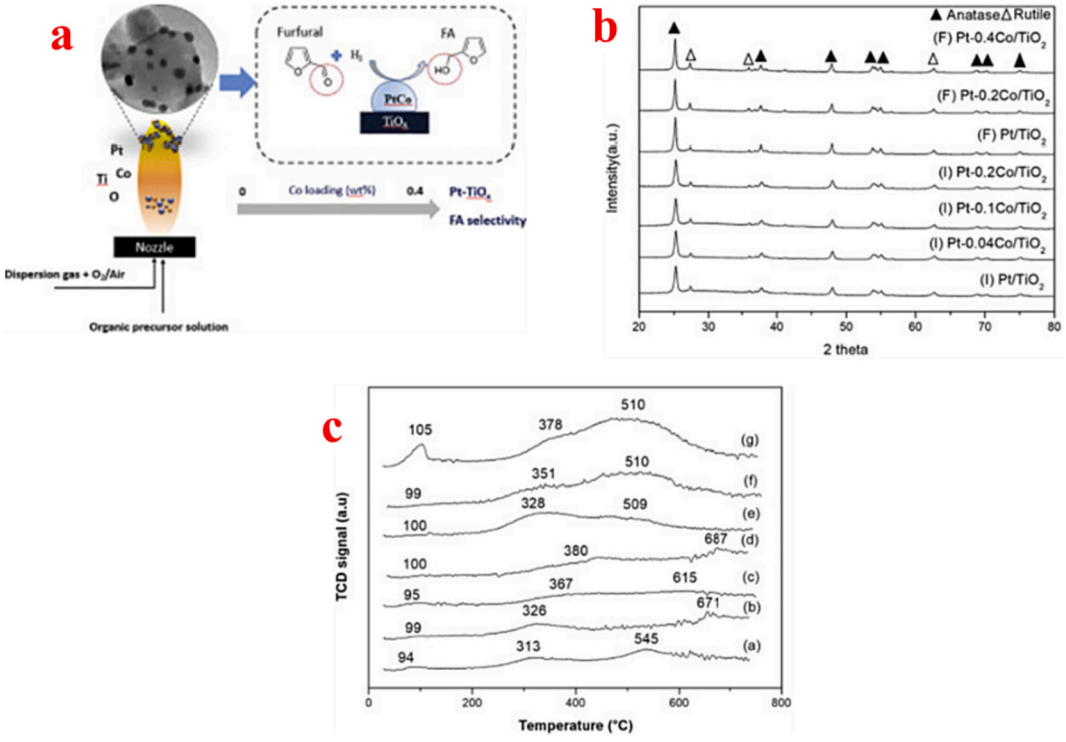

Fig. 20. Flame spray pyrolysis and the mechanism of hydrogenation of furfural (a) XRD patterns of the Pt-based catalysts synthesized by flame spray pyrolysis and impregnation techniques (b), and H_2-TPR profiles of various catalysts (c) [269].

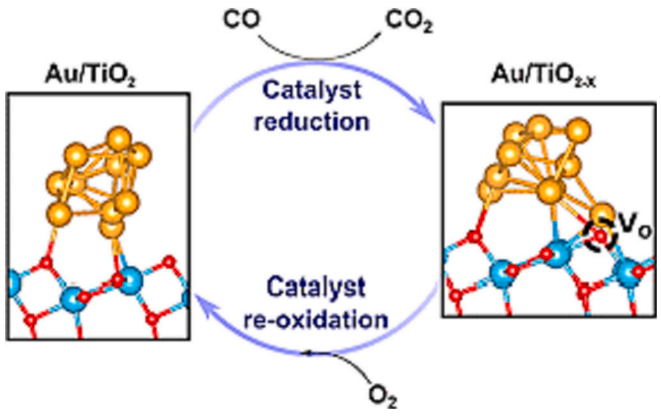

Fig. 21. CO oxidation mechanism over Au/TiO_2 catalyst [273].

interest due to their excellent activity at low temperatures, Pt catalysts are equally advantageous for the same catalytic reaction, especially when Pt is supported on the reducible oxides like TiO_2 [277] or FeO_x [278]. As a result, supported noble metal-catalysts are commonly employed in the catalytic oxidation of CO as a representative heterogeneous catalytic reaction owing to their superior catalytic activity [279]. The preparation process is equally important for the performance of supported noble metal catalysts as the design and regulation of their structure [280]. Nowadays, coprecipitation, sedimentation, and colloidal precipitation are some of the wet processes used to manufacture most laboratory-produced catalysts. These techniques need several time and energy-consuming posttreatment steps (filtration, drying, and calcination) to prepare the noble metal-based alloys like Ag—Pt [281], Au—Pt [282], and Pt—Pd [283]. On the other hand, the flame technique can quickly and cheaply prepare many supported catalysts since it is scalable, continuous, and quick. Recently, the flame spray pyrolysis technique has been applied for the synthesis of various supported metal oxide catalysts [284]. Jiang and his team loaded bimetallic Pt—Au nanoalloys on TiO_2 using one-step flame spray pyrolysis (Fig. 22a) as an efficient catalyst for CO oxidation at low temperatures [285]. XRD patterns showed the existence of a dual phase of titania (anatase and rutile), in addition, diffraction peaks for Au and Pt also exist in the XRD patterns of Pt_xAu_y nanocomposites (Fig. 22b). Among these prepared catalysts, $Pt_{0.75}Au_{0.25}$ exhibited the highest activity for CO oxidation at low temperatures (Fig. 22c), as well as long-term stability and no CO poisoning for 1000 min (Fig. 23a). XPS results showed three pairs of peaks for Pt that were mainly ascribed to Pt metal state and $Pt^{2+,}$ and Pt^{4+} oxidation states, respectively (Fig. 23b). Most likely, the oxidizing flame spray pyrolysis procedure at high-temperature generated the Pt partially oxidized species. However, the XPS spectra of Au 4f (Fig. 23c) shows peaks located at 83.0 and 86.7 eV, indicating the species are present in the metallic Au form. The NP alloy seems to be heavily charged negatively as compared to Pt and Au foils, which can be explained by the charge transfer from TiO_2 to metal centers and the formation of metal-support interactions.

Meanwhile, all the Pt spectra exhibited shift towards lower binding energies with decrease in platinum content varying from x = 1.0 to 0.25 with the insertion of Au. These findings may point to the development of metallic links between Au and Pt in the Pt—Au alloy. Or to put it another way, the existence of metallic bonds causes the extra e^- on Au atoms to migrate towards the nearby Pt atoms. According to the results obtained from in-situ DRIFTS spectra (Fig. 23d), a little shift for 2087 cm^{-1} sites to the lower energy, may result due to the e^- transfer from Au to Pt atoms. Finally, the strong contact of metal-support and e^- shift between Au and Pt in the alloy, work together synergistically to reduce CO's poisoning impact and increase its catalytic oxidation performance at low temperatures. Bi et al. increased thermal stability in case of Pt/TiO_2 through an in-situ N-surface doping technique utilizing flame spray pyrolysis and employed for CO oxidation [286]. Their research showed the presence of nitrogen atoms mostly concentrated on the catalyst's surface due to incorporation in the interstitial sites in the Ti-O-N and/or Ti-N-O lattice. Additionally, N-doped Pt/TiO_2 displayed greater stability as compared to the pure Pt/TiO_2 after being calcined at a range of temperatures (300–600 °C). This phenomenon can be primarily

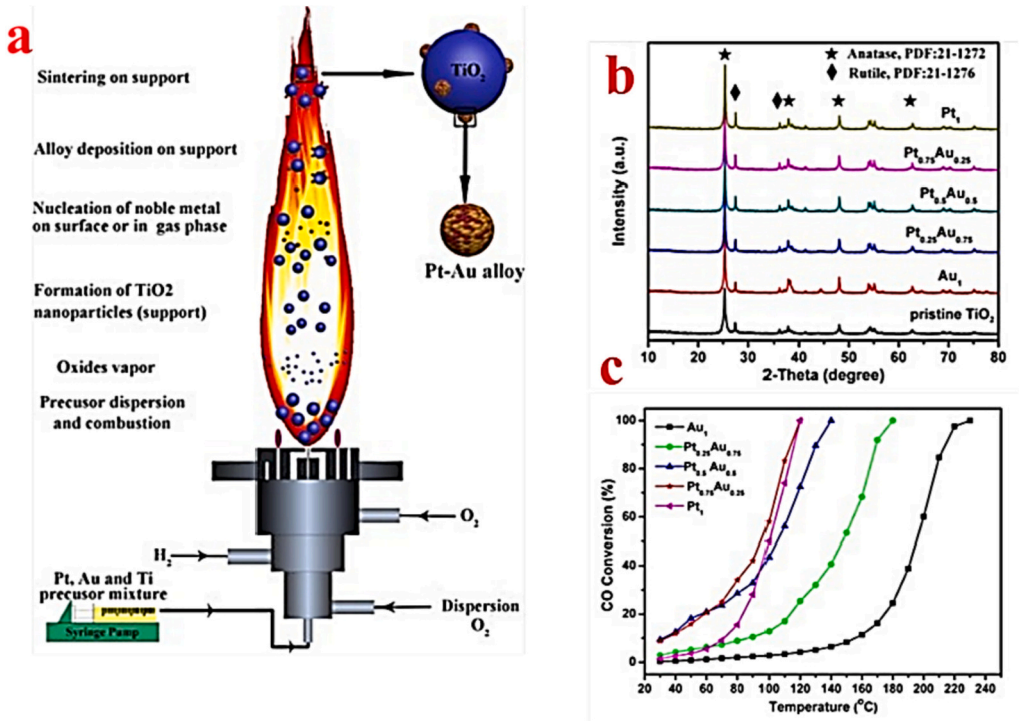

Fig. 22. Schematic presentation of FSP for the synthesis of Pt—Au supported TiO_2 catalysts (a) XRD patterns of flame-synthesized Pt_xAu_y nanocomposites (b) and catalytic activity of various Pt_xAu_y nanocomposites for CO oxidation (c) [285].

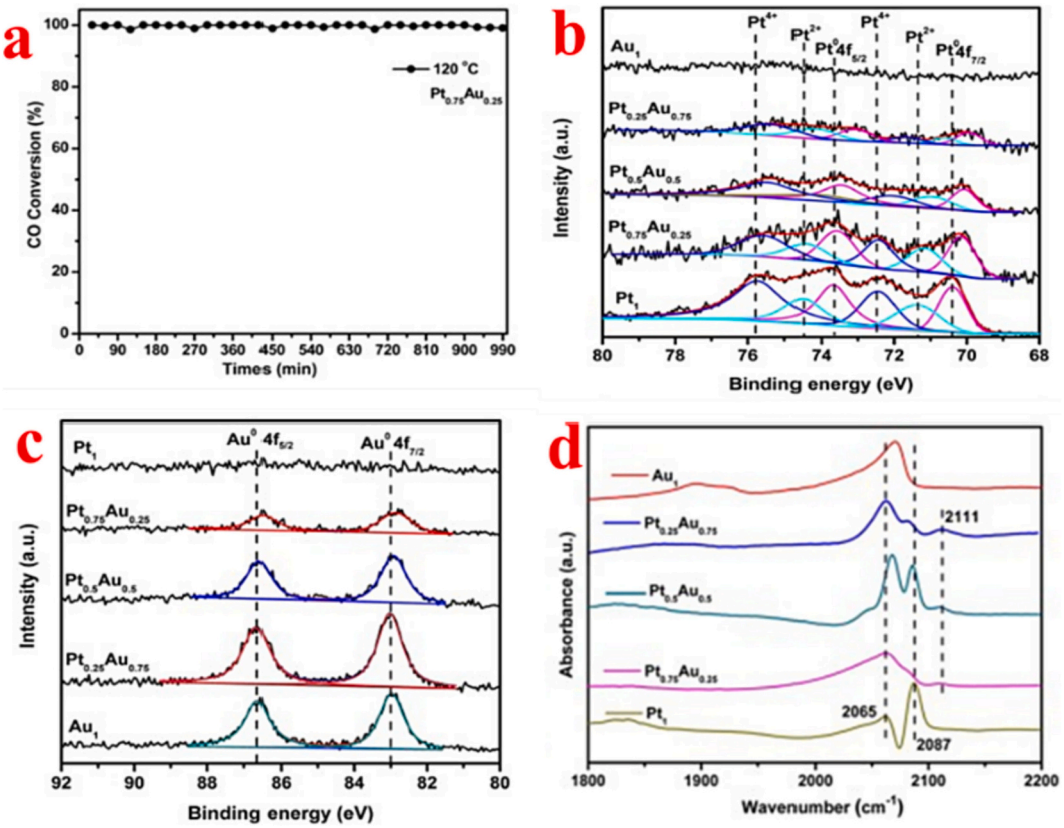

Fig. 23. Catalytic stability of $Pt_{0.75}Au_{0.25}$ catalysts (a) XPS spectra for Pt_xAu_y nanocomposites: Pt 4f (b), Au 4f (c), and in situ DRIFT spectra for all materials after Ar purged (10 min) (d) [285].

attributed to the creation of stronger Pt—N bonds, which enhances the resistance to sintering and minimizes phase transition during the calcination process. As previously stated, supported noble metal catalysts for catalytic combustion applications show great reaction activity and stability. Thus, the creation of inexpensive, effective, and earth-abundant catalysts is of special importance given the few resources and high price of noble metals. Due to their comparatively high catalytic performance and low price, copper-based catalysts have emerged as promising candidates [287]. Nevertheless, pristine copper-based catalysts are less stable and active than those made of noble metals [288]. Hence, it is practical to increase the stability and reactivity of these catalysts by adding various supports to the catalyst system [289]. The more typical supports are CeO_2, TiO_2, ZrO_2, and others. TiO_2 stands out among them and exhibits a positive impact on the catalysts' activity owing to its exceptional oxygen storage ability [290]. Moreover, metal oxide supported on TiO_2 can achieve improved stability as well as dispersion thanks to the strong metal-support interaction effect [291]. Chen and his team synthesized CuO-TiO_2 nanoparticles utilizing the flame spray pyrolysis (FSP) approach with varying mass concentrations of CuO (2–20%) and utilized for catalytic oxidation of lean CO at 120 °C [292]. The FSP approach may significantly increase CuO loading compared to other standard techniques without leaving behind big crystalline particles of CuO on the catalyst's surface. Besides, at elevated flame temperatures, copper cations are incorporated into the TiO_2 lattice and induce the transformation from anatase to rutile phase by generating oxygen defects. Furthermore, the interactions of CuO with TiO_2 significantly affects the physicochemical characteristics of the material. Finally, the presence of loaded CuO in the composite leads increased proportion of the more stable rutile phase in the material, consequently reducing the strong metal-support interaction that affects both the CuO and anatase phase. This modification enhances the CO catalytic combustion capabilities. Besides, the monometallic copper catalyst, the catalyst based on both copper and manganese presents remarkable CO and CH_4 catalytic activity, and they may eventually replace precious metal catalysts [293]. In heterogeneous catalysis, bimetallic nanocatalysts offer several advantages over their monometallic counterparts. The combination of two transition metals in a bimetallic catalyst creates unique electronic and structural properties that can enhance catalytic performance. The synergistic interaction between the two metals leads to improved catalytic activity, selectivity, and stability, surpassing the capabilities of individual metals [294]. Yuan and his colleagues supported TiO_2 with varying molar proportions of Cu and Mn mixed oxides by flame spray pyrolysis technique (Fig. 24a) and applied this catalyst in catalytic oxidation of lean CH_4 and CO (Fig. 24b) [295]. Among different bimetallic prepared catalysts, Cu − Mn/TiO_2 having 12 mol% loading showed the optimum catalytic activity for catalytic oxidation of CH_4 and CO during both temperature stages (low and high) (Fig. 25a-d). This increased catalytic activity is mainly attributed to the small particle size (Fig. 26a), high dispersion of cation oxide species (Fig. 26b-e), the higher $Mn^{4+} - O_{ads}$ and Cu^{1+}/Cu ratios of Lewis acid−base pairs (Fig. 27a), and conversion from anatase to rutile phase (Fig. 27b&c).

4. Summary and outlook

TiO_2 as a catalyst and photocatalyst material has been intensively studied in the last decades due to its high activity, stability, availability, and ease of synthesis. Nevertheless, its wide-scale applications were greatly restricted because of its wide band gap, and more charge recombination rates. Numerous initiatives, such as metal and non-metal doping, heterostructure composites, the synthesis of nanomaterials with porous structures, and the development of synthesis techniques, were made to resolve these problems. Understanding and modifying synthesis techniques, as well as the variables and settings that result in the

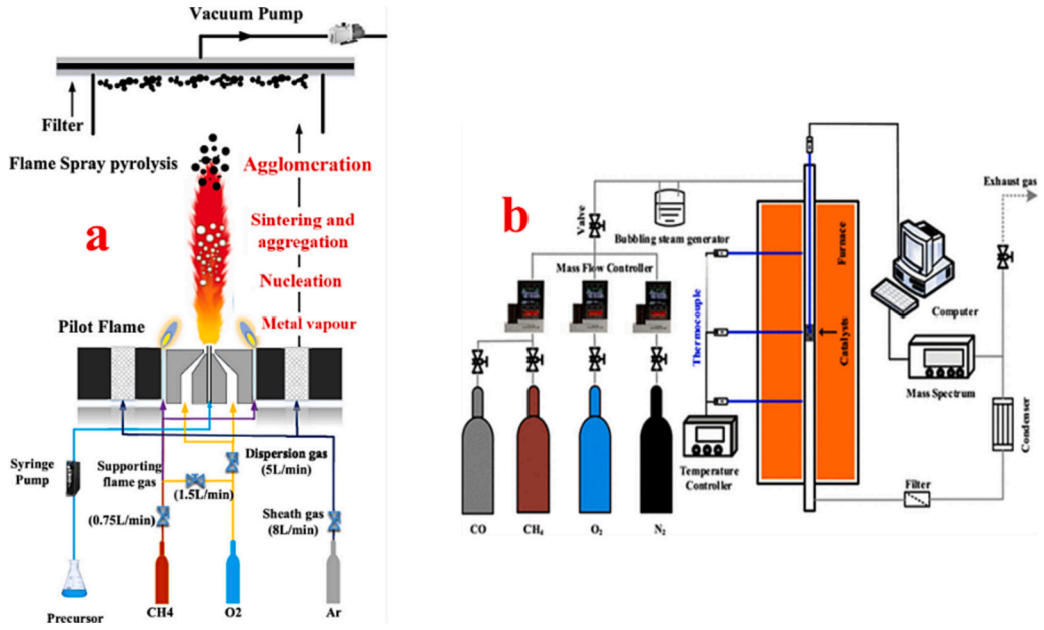

Fig. 24. Sketch for the FSP used for the synthesis of catalysts (a) and Experimental setup for the catalytic combustion (b) [295].

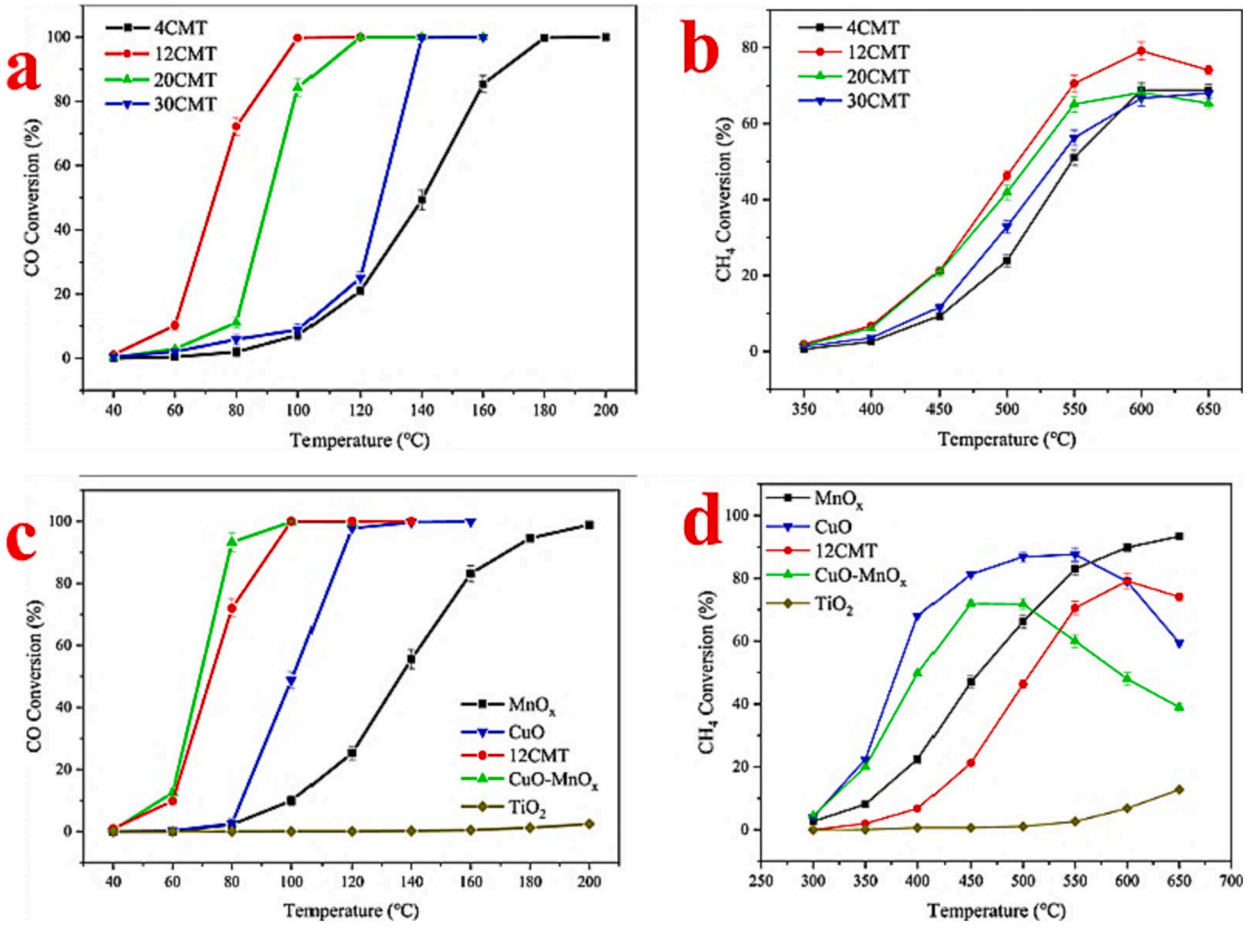

Fig. 25. Photocatalytic activity performance over Cu − Mn/TiO_2 nanoparticles for oxidation of CO (a) and CH_4 (b), photocatalytic evaluation curves over different Cu − Mn/TiO_2 nanoparticles compared to MnO_2, CuO, and TiO_2 for catalytic oxidation of CO (c), and CH_4 (d) [295].

preparation of highly active photocatalyst material, is therefore crucial for producing a photocatalyst with superior catalytic activity for different variety of applications. Flame spray pyrolysis is the most popular method for producing nanomaterials on a large commercial scale and has been extensively investigated to create catalysts over the past 20 years. Numerous investigations have shown that flame spray

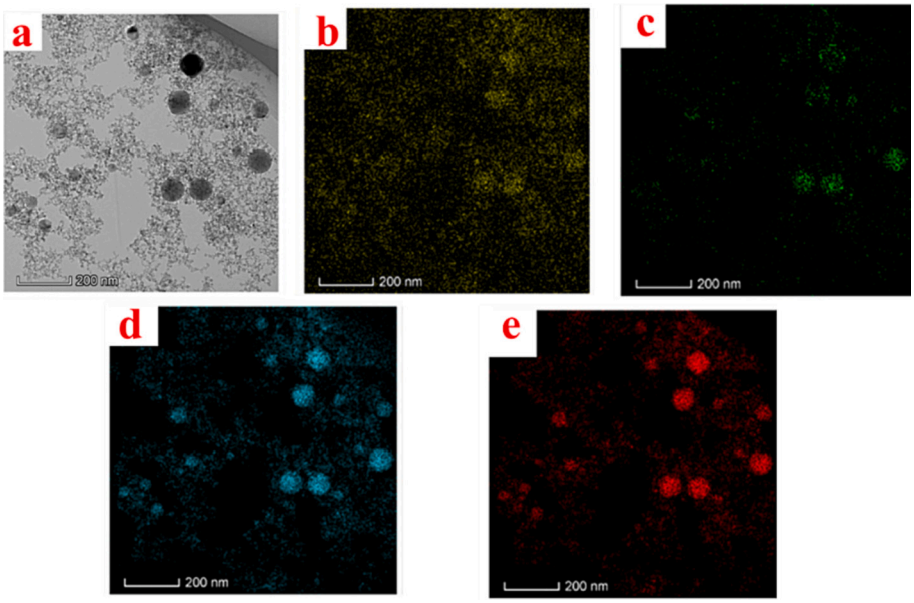

Fig. 26. TEM (a) and EDX of 12Cu − Mn/TiO_2 catalyst: Cu (b), Mn (c), O (d), and Ti (e) [295].

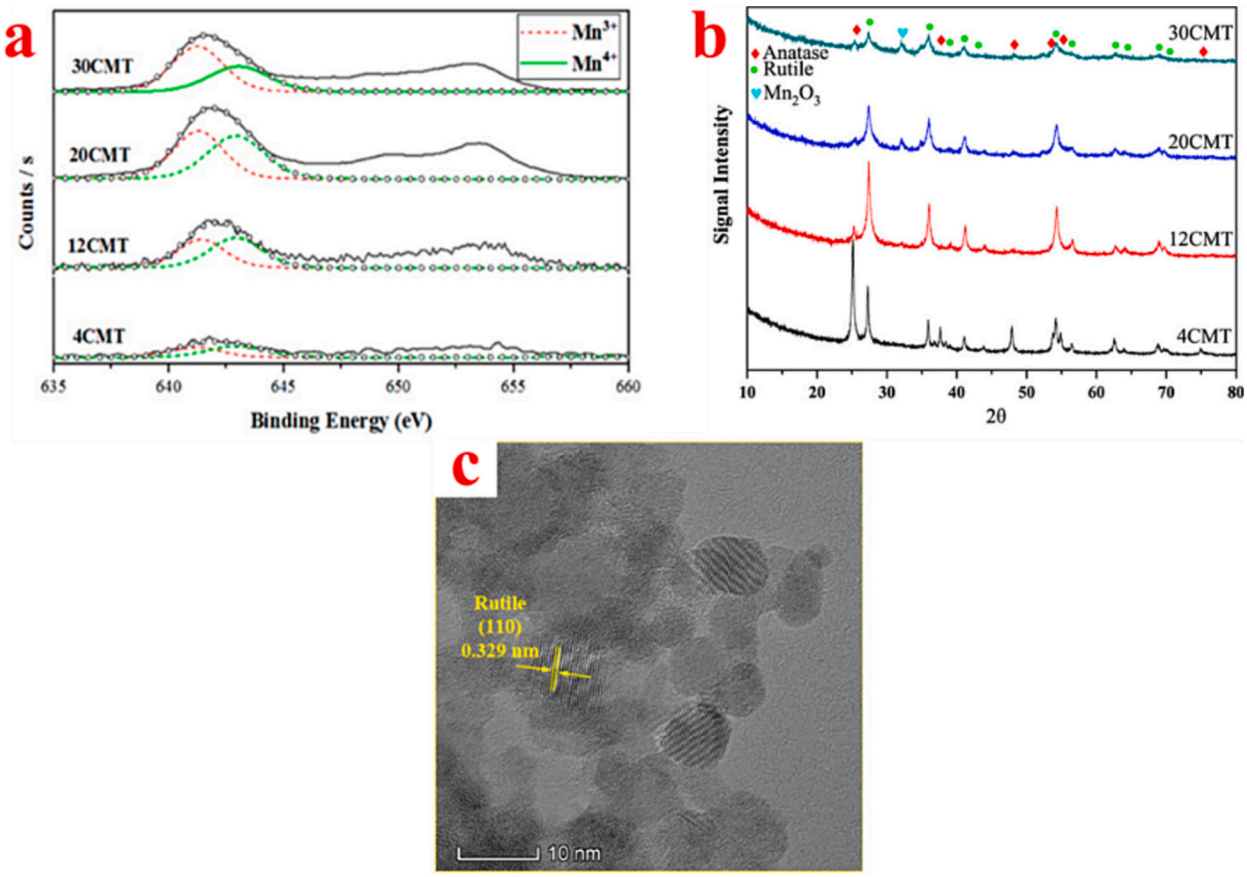

Fig. 27. XPS of Mn for Cu − Mn/TiO_2 (a) XRD patterns of various catalysts (b), and HRTEM for 12Cu − Mn/TiO_2 catalyst, representing the rutile phase [295].

pyrolysis could offer beneficial chances to produce distinctive nano-catalysts that are inaccessible by conventional wet chemistry techniques such as impregnation and sol-gel methods. Among these investigations, doping with noble or transition metals can be considered as a promising route in enhancing the catalytic performance of TiO_2. Although this technique can be achieved using conventional synthesis methods, with FSP, the obtained materials should have better performance and effeciency due to the formation of porous structure, enlarged surface area, and better metals distribution. This approach gives users the ability to tailor the catalytic characteristics by precisely controlling the process parameters which control allows for the systematic design of catalysts towards the best possible structure and function. This method's limited

number of continuous manufacturing processes enables scalable production with dependable physicochemical properties. The primary focus of this review article was to examine and analyze the synthesis of TiO_2-based materials for a variety of catalytic applications including organic transformation (hydrogenation of 3-nitrostyrene, 1-hyptene, and furfural, and catalytic oxidation of CO), photocatalysis (decontamination of organics, photocatalytic water splitting, CO_2 photoreduction), thermocatalytic (CO_2 methanation, and removal of VOCs) applications, and electrocatalysis. Nevertheless, there are still some challenges with this technology:

1. The cost of manufacturing increases with the use of expensive organic precursor solvents, whereas the spray flame pyrolysis reactor utilizes less expensive water precursors, but frequently generates inhomogeneous particles.
2. Its applicability is sometimes constrained by the creation of less crystalline and non-porous nanoparticles.
3. To address these challenges, we shouldn't just focus on a reaction's final catalytic performance. It is strongly advised to do more in-depth in situ characterization studies in order to comprehend how catalysts arise during flame spray pyrolysis and to build more advanced flame reactors.
4. Recently, several research have been done on the synthesis of various nanocatalytic materials using flame spray pyrolysis for applications in energy and environmental issues, most of these produced nanomaterials are deposited onto silica support. Thus, many efforts were put into increasing the catalytic activity by doping other elements to have synergistic effects, increasing the surface area, or dispersing the catalytic activity.
5. Most of the published papers are focused on catalytic and photocatalytic activity of common oxide nanomaterials like ZnO, and TiO_2 that are synthesized using this technique, however, application of this method to synthesize other nanomaterials like g-C_3N_4, perovskite, and mixed metal oxides are also recommended.

Besides, the following points should be considered for the technology roadmap and perspectives of the FSP technology:

1. The characterization of the ideal precursor-solvent combination should be considered including the stability at room temperature, obtained from low-cost and available recycled materials, high solubility within the solvent, and if it can be powered by renewable sources of energy for more sustainable nanoparticle production.
2. It would be beneficial to create computational modeling of individual precursor-solvent droplets in order to accurately forecast the commencement of droplet micro-explosion and, consequently, identify the preferred conversion pathway for a particular precursor-solvent mixture.
3. Optimizing reactor design and guiding the best possible choice of appropriate chemicals for experimental screening studies in flame spray synthesis can be achieved by automatically calculating most likely mechanisms, reaction rate transport, and solubility properties, as well as by finding precursor-solvent libraries.
4. The experimental diagnostics for flame sprays, aerosols, and nanoparticles by referencing the most recent developments was evaluated in over 20 distinct characterization methodologies. To conduct a thorough FSP reactor study, a variety of techniques should preferably be combined into a single setup to enable quick examinations of the pertinent process variables (such as reactor types, feed rates, precursor–solvent combinations, etc.). This makes it possible to quickly acquire data libraries for validating models.

Finally, besides catalysts and photocatalysts, flame spray pyrolysis also finds applications in different areas like sensors [296], electrode materials [297], photoanode [298], and bioimaging [299]. These fields are also highly recommended for future research beyond catalyst and photocatalyst applications. We anticipate that the manufacture of catalytic nanoparticles will play a significant part in the growth of the significance of flame-made nanomaterials in the future as a key technique for the scalable fabrication of sophisticated nanomaterials for use in a variety of fields.

Authors contribution

Mohammed Ismael (the corresponding author in the manuscript) collected all the scientific data and wrote most sections of the manuscript. Sharma and Kumar enriched the scientific contact and improved the whole manuscript.

CRediT authorship contribution statement

Mohammed Ismael: Data curation, Investigation, Supervision, Writing – original draft. **Anuradha Sharma:** Conceptualization, Visualization, Writing – review & editing. **Naveen Kumar:** Conceptualization, Visualization, Writing – review & editing.

Declaration of competing interest

The author affirms that they have no known financial or interpersonal conflicts that would have looked to have an impact on the work disclosed in this review.

Data availability

Data will be made available on request.

References

[1] M. Armand, J.M. Tarascon, Nature. 451 (2008) 652–657.
[2] J.B. Goodenough, K.S. Park, J. Am. Chem. Soc. 135 (2013) 1167–1176.
[3] N. Armaroli, V. Balzani, Energy Environ. Sci. 4 (2011) 3193–3222.
[4] M. Höök, X. Tang, Energy Policy 52 (2013) 797–809.
[5] L. Zhou, Z. Zhuang, H. Zhao, M. Lin, D. Zhao, L. Mai, Adv. Mater. 29 (2017) 1602914.
[6] Y. Zheng, J. Wang, B. Yu, W. Zhang, J. Chen, J. Qiao, J. Zhang, Chem. Soc. Rev. 46 (2017) 1427–1463.
[7] D.P. Sahoo, D. Rath, B. Nanda, K.M. Parida, RSC Adv. 5 (2015) 83707–83724.
[8] Q.J. Xiang, B. Cheng, J.G. Yu, Angew. Chem. Int. Ed. 54 (2015) 11350–11366.
[9] M.N. Gupta, Renew. Sust. Energ. Rev. 71 (2016) 585–601.
[10] R. Kothari, D. Buddhi, L.R. Sawhney, Renew. Sust. Energ. Rev. 12 (2) (2008) 553–563.
[11] H. Balat, E. Kirtay 35 (14) (2010) 7416–7426.
[12] I. Dincer, C. Acar, Int. J. Hydrog. Energy 40 (2015) 11094–11111.
[13] B. Zhang, S.X. Zhang, R. Yao, Y.H. Wu, J.S. Qiu, J. Electron. Sci. Technol. 19 (2021) 100080.
[14] Y.S. Tee, Y.K. Win, S.W. Teo, D.L. Koh, S. Liu, P.C. Teng, et al., Adv. Sci. 4 (2017) 1600337.
[15] C. Acar, I. Dincer, Int. J. Energy Res. 39 (2015) 1757–1768.
[16] J. Zhu, M. Zach, Curr Opin colloid, Interf. Sci. 14 (2009) 260–269.
[17] N. Muradov, T. Veziroglu, Int. J. Hydrog. Energy 33 (2008) 6804–6839.
[18] M. Ismael, E. Elhaddad, M. Wark, Coll. Surf. A Physicochem. Eng. Asp. 638 (2022) 128288.
[19] M. Ismael, Y. Wu, M. Wark, New J. Chem. 43 (2019) 4455.
[20] M. Ismael, J. Environ. Chem. Eng. 8 (2020) 103676.
[21] T. Zhang, K. Zhao, J. Yu, J. Jin, Y. Qi, H. Li, X. Hou, G. Liu, Nanoscale. 5 (2013) 8375–8383.
[22] M. Ismael, Mater. Res. Bull. 151 (2022) 111803.
[23] M. Ismael, M. Wark, Flat Chem. 32 (2022) 100337.
[24] M. Ismael, J. Alloys Compd. 846 (2020) 156446.
[25] B.Y. Guan, X.Y. Yu, H.B. Wu, X.W.D. Lou, Adv. Mater. 29 (2017) 1706314.
[26] W. Xia, A. Mahmood, R. Zou, Q. Xu, Energy Environ. Sci. 8 (2015) 1837–1866.
[27] S. Rashidi, J.A. Esfahani, A. Rashidi, Renew. Sust. Energ. Rev. 73 (2017) 1198–1210.
[28] H.H. Ou, S.L. Lo, Sep. Purif. Technol. 58 (2007) 179–191.
[29] M. Ismael, D.H. Taffa, E. Elhaddad, M. Wark, Catalysts. 7 (2017) 326.
[30] M. Ismael, D.H. Taffa, E. Elhaddad, M. Wark, Catal. Today 313 (2018) 47–54.
[31] M. Ismael, M. Wark, Catalysts. 9 (2019) 342.
[32] M. Ismael, New J. Chem. 43 (2019) 13783–13793.
[33] M. Ismael, New J. Chem. 43 (2019) 9596.
[34] M. Ismael, Chem. Phys. Lett. 739 (2020) 136992.
[35] A.R. Studart, U.T. Gonzenbach, E. Tervoort, L.J. Gauckler, J. Am. Chem. Soc. 89 (2006) 1771–1789.

[36] J. Maier, Angew. Chem. 52 (2013) 4998–5026.
[37] F. Zhang, X. Wang, H. Liu, C. Liu, Y. Wan, Y. Long, Z. Cai, Catalysts. 9 (12) (2019) 2489.
[38] S.H. Choi, Y.C. Kang, Carbon. 79 (2014) 58–66.
[39] R. Koirala, S.E. Pratsinis, A. Baiker, Chem. Soc. Rev. 45 (2016) 3053–3068.
[40] W.Y. Teoh, Materials. 6 (2013) 3194.
[41] W.Y. Teoh, R. Amal, L. Mädler, Nanoscale. 2 (2010) 1324–1347.
[42] S. Li, Y. Ren, P. Biswas, S.D. Tse, Prog. Energy Combust. Sci. 55 (2016) 1–59.
[43] S. Venkatesan, J. Mitzel, K. Wegner, R. Costa, P. Gazdzicki, K.A. Friedrich, Renew. Sust. Energ. Rev. 158 (2022) 112080.
[44] H. Chen, H.K. Mulmudi, A. Tricoli, Chin. Chem. Lett. 31 (2020) 601–604.
[45] S. Li, Y. Ren, P. Biswas, S.D. Tse, Prog. Energy Combust. Sci. 55 (2016) 1–59.
[46] G.A. Kelesidis, E.G. Sotiris, E. Pratsinis, Proc. Combust. Inst. 36 (1) (2017) 29–50.
[47] W.Y. Teoh, R. Amal, L. Mädler, Nanoscale. 2 (2010) 1324–1347.
[48] Y. Zhu, Z. Xu, K. Yan, H. Zhao, J. Zhang, ACS Appl. Mater. Interfaces 9 (46) (2017) 40452–40460.
[49] K.K. Akurati, A. Vital, G. Fortunato, R. Hany, F. Nueesch, T. Graule, Solid State Sci. 9 (3) (2007) 247–257.
[50] L. Mädler, H. Kammler, R. Mueller, J.E.S. Pratsinis, Aerosol. Sci. 33 (2) (2022) 369–389.
[51] F. Gao, Z. Xu, H. Zhao, Proc. Combust. Inst. 38 (2021) 6503–6511.
[52] K. Itatani, R. Yasuda, F.S. Howell, A. Kishioka, J. Mater. Sci. 32 (1997) 2977–2984.
[53] A.S. Edelstien, R.C. Cammarata (Eds.), Nanomaterials—Synthesis, Properties and Applications, IOP Publishing Ltd, London, UK, 1996.
[54] A. Tricoli, N. Nasiri, H. Chen, A.S. Wallerand, M. Righettoni, Sol. Energy 136 (2016) 553–559.
[55] E.K. Athanassiou, R.N. Grass, W.J. Stark, Aerosol Sci. Technol. 44 (2010) 161–172.
[56] R. Wallace, A.P. Brown, R. Brydson, K. Wegner, S.J. Milne, J. Mater. Sci. 48 (2013) 6393–6403.
[57] S. Phanichphant, C. Liewhiran, K. Wetchakun, A. Wisitsoraat, A. Tuantranont, Sensors. 11 (2011) 472–484.
[58] R.M. Laine, J.C. Marchal, H.P. Sun, X.Q. Pan, Nat. Mater. 5 (2006) 710–712.
[59] S. Rajput, L.P. Singh, C.U. Pittman Jr., D. Mohan, J. Colloid Interface Sci. 492 (2017) 176–190.
[60] S. Sel, O. Duygulu, U. Kadiroglu, N.E. Machin, Appl. Surf. Sci. 318 (2014) 150–156.
[61] A. Tricoli, M. Graf, S.E. Pratsinis, Adv. Funct. Mater. 18 (2008) 1969–1976.
[62] Y. Liu, J. Huang, Y. Gong, X. Xu, H. Li, Ceram. Int. 43 (2017) 13185–13192.
[63] S. Pokhrel, J. Birkenstock, M. Schowalter, A. Rosenauer, L. Mädler, Cryst. Growth Des. 10 (2010) 632–639.
[64] O. Arutanti, A.B.D. Nandiyanto, T. Ogi, F. Iskandar, T.O. Kim, K. Okuyama, J. Alloys Compd. 591 (2014) 121–126.
[65] C. Siriwong, N. Wetchakun, C. Liewhiran, S. Phanichphant, AIP Conference Proceedings 1151, American Institute of Physics, 2009, pp. 13–16.
[66] R. Strobel, S.E. Pratsinis, J. Mater. Chem. 17 (2007) 4743–4756.
[67] T. Rudin, K. Wegner, S.E. Pratsinis, J. Nanopart. Res. 13 (2011) 2715–2725.
[68] K.B. Riad, P.M. Wood-Adams, K. Wegner, Mater. Res. Bull. 106 (2018) 276–281.
[69] P. Vivek, J. Chandrasekaran, V. Balasubramani, Sens. Actuator A Phys. 335 (2022) 113361.
[70] B. Sun, S. Pokhrel, D.R. Dunphy, H. Zhang, Z. Ji, X. Wang, M. Wang, Y.P. Liao, C. H. Chang, J. Dong, R. Li, L. Mädler, C.J. Brinker, A.E. Nel, T. Xia, ACS Nano 9 (9) (2015) 9357–9372.
[71] G. Kühner, M. Voll, In Carbon Black, ed. J. B. Donnet, R. C. Bansal and M. J. Wang, Marcel Dekker, New York, 2nd edn, 1993, p. 1.
[72] Y. Ding, X. Ma, X. Zhang, J. Alloys Compd. 959 (2023) 170540.
[73] R. Strobel, A. Baiker, S.E. Pratsinis, Adv. Powder Technol. 17 (2006) 457.
[74] A. Camenzind, R. Strobel, F. Krumeich, S.E. Pratsinis, Adv. Powder Technol. 18 (2007) 5.
[75] T. Sahm, L. Mädler, A. Gurlo, N. Barsan, S.E. Pratsinis, U. Weimar, Sensors Actuators B Chem. 98 (2004) 148.
[76] S. Loher, W.J. Stark, M. Maciejewski, A. Baiker, S.E. Pratsinis, D. Reichardt, F. Maspero, F. Krumeich, D. Gunther, Chem. Mater. 17 (2005) 36.
[77] D. Li, W.Y. Teoh, C. Selomulya, R.C. Woodward, R. Amal, B. Rosche, Chem. Mater. 18 (2006) 6403.
[78] F.O. Ernst, H.K. Kammler, A. Roessler, S.E. Pratsinis, W.J. Stark, U. Ufheil, P. Novak, Mater. Chem. Phys. 101 (2007) 372.
[79] A.C. Sutorik, M.S. Baliat, Mater. Sci. Forum 386–388 (2002) 371.
[80] J. Harra, S. Kujanpää, J. Haapanen, P. Juuti, M.J. Mäkelä, L. Hyvärinen, M. Honkanen, AICHE J. 63 (2017) 881–892.
[81] R. Strobel, E.S. Pratsinis, Phys. Chem. Chem. Phys. 13 (2011) 9246–9252.
[82] C. Abram, M. Mezhericher, F. Beyrau, A.H. Stone, Y. Ju, Y. Proc. Combust Inst. 37 (2019) 1231–1239.
[83] R. Strobel, F. Krumeich, W.J. Stark, S.E. Pratsinis, A. Baiker, J. Catal. 222 (2004) 307–314.
[84] O. Arutanti, F.A. Arif, R. Balgis, T. Ogi, K. Okuyama, F. Iskandar, AICHE J. 62 (2016) 3864–3873.
[85] R. Jossen, E.S. Pratsinis, J.W. Stark, et al., J. Am. Ceram. Soc. 88 (6) (2005) 1388–1393.
[86] J. Wei, S. Li, Y. Ren, Proc. Combust. Inst. 37 (1) (2019) 1193–1201.
[87] H. Li, D.C. Rosebrock, Y. Wu, et al., Proc. Combust. Inst. 37 (1) (2019) 1203–1211.
[88] F. Meierhofer, H. Li, M. Gockeln, R. Kun, T. Grieb, A. Rosenauer, U. Fritsching, J. Kiefer, J. Birkenstock, L. Mädler, S. Pokhrel, ACS Appl. Mater. Interfaces 9 (2017) 37760–37777.
[89] I. Skenderovic, G. Kotalczyk, F.E. Kruis, Dual population balance Monte Carlo simulation of particle synthesis by flame spray pyrolysis, Processes. 6 (2018) 253.
[90] R. Abe, J. Photochem. Photobiol. C 11 (2010) 179–209.
[91] M. Ismael, Fuel. 303 (2021) 121207.
[92] S. Kumar, S. Jain, B.Y. Lamba, P. Kumar, Sol. Energy 159 (2018) 423–433.
[93] S. Agrawal, N.J. English, K.R. Thampi, J. MacElroy, Phys. Chem. Chem. Phys. 14 (2012) 12044–12056.
[94] K. Nakata, A. Fujishima, J Photochem Photobiol C: Photochem Rev 13 (3) (2012) 169–189.
[95] M. Ismael, Sol. Energy Mater. Sol. Cells 219 (2021) 110786.
[96] W.Y. Teoh, L. Mädler, D. Beydounb, S.E. Pratsinis, R. Amal, Chem. Eng. Sci. 60 (2005) 5852.
[97] W.Y. Teoh, F. Denny, R. Amal, D. Friedmann, L. Mädler, S.E. Pratsinis, Top. Catal. 44 (2007) 489.
[98] G.L. Chiarello, E. Selli, L. Forni, Appl. Catal. B Environ. 84 (2008) 332–339.
[99] G.L. Chiarello, L. Forni, E. Selli, Catal. Today 144 (2009) 69–74.
[100] M. Bernareggi, M.V. Dozzi, L.G. Bettini, A.M. Ferretti, G.L. Chiarello, E. Selli, Catalysts. 7 (10) (2017) 301.
[101] R. Asahi, T. Morikawa, H. Irie, T. Ohwaki, Chem. Rev. 114 (2014) 9824.
[102] J.C. Colmenares, R.S. Varma, P. Lisowski, Green Chem. 18 (2016) 5736.
[103] X. Chen, S.S. Mao, Chem. Rev. 107 (2007) 2891.
[104] S.G. Babu, R. Vinoth, D.P. Kumar, M.V. Shankar, H.L. Chou, K. Vinodgopal, B. Neppolian, Nanoscale. 7 (2015) 7849.
[105] D. Ni, H. Shen, H. Li, Y. Ma, T. Zhai, Appl. Surf. Sci. 409 (2017) 241.
[106] F. Yang, M. Liu, X. Chen, Z. Xu, H. Zhao, Sol. RRL. 2 (2018) 1800215.
[107] Q. Wang, C. Chen, D. Zhao, W. Ma, J. Zhao, Langmuir. 24 (2008) 7338–7345.
[108] H.G. Yang, C.H. Sun, S.Z. Qiao, J. Zou, G. Liu, S.C. Smith, H.M. Cheng, C.Q. Lu, Nature 435 (2008) 638–641.
[109] G.L. Chiarello, M.V. Dozzi, M. Scavini, J.D. Grunwaldt, E. Selli, Appl. Catal. B: Catal. 160-161 (2014) 144–151.
[110] P. Fernandez-Ibanez, M. Polo-López, S. Malato, S. Wadhwa, J. Hamilton, P. Dunlop, R. D'sa, E. Magee, K. O'shea, D. Dionysiou, Chem. Eng. J. 261 (2015) 36–44.
[111] D. Chen, Y. Cheng, N. Zhou, P. Chen, Y. Wang, K. Li, S. Huo, P. Cheng, P. Peng, R. Zhang, L. Wang, H. Liu, Y. Liu, R. Ruan, J. Clean. Prod. 268 (2020) 121725.
[112] N. Morin-Crini, G. Crini, L. Roy, Eaux industrielles contaminées, J. PUFC Besançon. (2017) 513.
[113] G. Crini, E. Lichtfouse, D.L. Wilson, N. Morin-Crini, J. Environ. Chem. Lett. 17 (1) (2019) 195–213.
[114] Q. Gao, J. Xu, H.X. Bu, Coord. Chem. Rev. 378 (2019) 17–31.
[115] K. Vellingiri, P. Kumar, H.K. Kim, Nano Res. 9 (2016) 3181–3208.
[116] M. Wen, G. Li, H. Liu, J. Chen, T. An, H. Yamashita, Environ. Sci. Nano 6 (2019) 1006–1025.
[117] C. Chen, W. Ma, J. Zhao, Chem. Soc. Rev. 39 (2010) 4206–4219.
[118] E.M. Samsudin, S.N. Goh, T.Y. Wu, T.T. Ling, S.B.A. Hamid, J.C. Juan, Sains Malaysiana 44 (7) (2015) 1011–1019.
[119] M. Ismael, J. Environ. Chem. Eng. 10 (2022) 108640.
[120] T. An, L. Sun, G. Li, Y. Gao, G. Ying, Appl. Catal. B 102 (2011) 140–146.
[121] L.G. Bettini, M.V. Dozzi, F.D. Foglia, G.L. Chiarello, E. Selli, C. Lenardi, P. Piseri, P. Milani, Appl. Catal. B Environ. 178 (2015) 226–232.
[122] B. Sun, A.V. Vorontsov, P.G. Smirniotis, Langmuir. 19 (2003) 3151–3156.
[123] A.R. Wassel, M.E. El-Naggar, K. Shoueir, J. Environ. Chem. Eng. 8 (2020) 104175.
[124] T. Boningari, S.N. Reddy, I.M. Suidan, P.G. Smirniotis, Chem, Engl. J. 339 (2018) 249–258.
[125] J. Wang, D.N. Tafen, J.P. Lewis, Z. Hong, A. Manivannan, M. Zhi, M. Li, N. Wu, J. Am. Chem. Soc. 131 (2009) 12290–12297.
[126] R. Asahi, T. Morikawa, T. Ohwaki, K. Aoki, Y. Taga, Science. 293 (2001) 269–271.
[127] T. Xia, Y. Zhang, J. Murowchich, X. Chen, Catal. Today 225 (2014) 2–9.
[128] J. Huo, Y. Hu, H. Jiang, X. Hou, C. Li, Chem. Eng. J. 258 (2014) 163–170.
[129] P.G. Smirniotis, T. Boningari, D. Damma, S.N.R. Inturi, Catal. Commun. 113 (2018) 1–5.
[130] F.A. Unal, S. Ok, M. Unal, S. Topal, K. Cellat, F. Şen, J. Mol. Liq. 299 (2020) 112177.
[131] J.C.S. Wu, C.H. Chen, J. Photochem. Photobiol. A 163 (2004) 509–515.
[132] K.E. Karakitsou, X.E. Verykios, J. Phys. Chem. 97 (1993) 1184–1189.
[133] B. Grzybowska, J. Słoczynski, R. Grabowski, K. Samson, I. Gressel, K. Wcisło, L. Gengembre, Y. Barbaux, Appl. Catal. A Gen. 230 (2002) 1–10.
[134] B. Tian, C. Li, F. Gu, H. Jiang, Y. Hu, J. Zhang, Chem, Engl. J. 151 (2009) 220–227.
[135] Z.L. Liu, Z.L. Cui, Z.K. Zhang, Mater. Charact. 54 (2005) 123–129.
[136] I. Khan, A. Yuan, A. Khan, S. Khan, S. Khan, S.A. Shah, W. Yaseen, Y. Cui, X. Shen, X. Wang, Surf Interf. 34 (2022) 102358.
[137] B. Tian, C. Li, J. Zhang, Chem. Eng. J. 191 (2012) 402–409.
[138] Y. Furubayashi, T. Hitosugi, Y. Yamamoto, K. Inaba, G. Kinoda, Y. Hirose, T. Shimada, T. Hasegawa, Appl. Phys. Lett. 86 (2005) 252101.
[139] X. Niu, W. Yan, H. Zhao, J. Yang, Appl. Surf. Sci. 440 (2018) 804–813.
[140] B. Mei, M.D. Sánchez, T. Reinecke, S. Kaluza, W. Xia, M. Mühler, J. Mater. Chem. 21 (2009) 11781–11790.
[141] C.D. Valentin, G. Pacchioni, J. Phys. Chem. C 113 (2009) 20543–20552.
[142] K.A. Michalow, D. Flak, A. Heel, M. Parlinska-Wojtan, M. Rekas, T. Graule, Environ. Sci. Pollut. Res. 19 (2012) 3696–3708.
[143] R. Marschall, Adv. Funct. Mater. 24 (2014) 2421–2440.
[144] K. Saito, E. Yi, R.M. Laine, Y. Sugahara, Ceram. Int. 46 (2020) 1314–1322.
[145] Y. Jiang, J. Scott, R. Amal, Appl. Catal. B Environ. 126 (2012) 290–297.

[146] M. Addamo, V. Augugliaro, S. Coluccia, M.G. Faga, E. García-López, V. Loddo, G. Marcì, G. Martra, L. Palmisano, J. Catal. 235 (2005) 209–220.
[147] S.N.R. Inturi, T. Boningari, M. Suidan, P.G. Smirniotis, Appl. Catal. B Environ. 144 (2014) 333–342.
[148] W.Y. Teoh, R. Amal, L. Mädler, S.E. Pratsinis, Catal. Today 120 (2007) 203–213.
[149] T. Hirasawa, J.C. Sung, Z. Yang, A. Joshi, H. Wang, Combust. Flame 139 (2004) 288–299.
[150] K.A. Shah, B.A. Tali, Mater. Sci. Semicond. Process. 41 (2016) 67–82.
[151] A.R. Afre, T. Soga, T. Jimbo, M. Kumar, Y. Ando, M. Sharon, Chem. Phys. Lett. 414 (2005) 6–10.
[152] D.B.A. Nandiyanto, Y. Kaihatsu, F. Iskandar, K. Okuyama, Mater. Lett. 63 (2009) 1847–1850.
[153] D.L. Hafshejani, S. Tangsir, H. Koponen, J. Riikonen, T. Karhunen, U. Tapper, P. V. Lehto, H. Moazed, A.A. Naseri, A. Hooshmand, Powder Technol. 298 (2016) 42–49.
[154] N.S. Inamdar, K.S. Haram, J. Nanosci. Nanotechnol. 6 (2006) 2155–2158.
[155] I. Hod, W. Bury, D.M. Gardner, P. Deria, V. Roznyatovskiy, M.R. Wasielewski, O. K. Farha, J.T. Hupp, J. Phys. Chem. Lett. 6 (4) (2015) 586–591.
[156] M.A. Ismail, M.N. Hedhili, D.H. Anjum, V. Singaravelu, S.H. Chung, Catalysts. 11 (4) (2021) 438.
[157] W. Bia, Y. Hua, H. Jiang, H. Yu, W. Li, C. Li, Appl. Surf. Sci. 481 (2019) 360–368.
[158] C. Jiang, H. Wang, Y. Wang, C. Xue, Z. Yang, C. Yu, H. Ji, J. Hazard. Mater. 390 (2020) 122182.
[159] X. Wan, L. Wang, S. Gao, X. Lang, L. Wang, T. Zhang, A. Dong, W. Wang, Chem. Eng. J. 410 (2021) 128305.
[160] J. Kong, Z. Xiang, G. Li, T. An, Appl. Catal. B Environ. 269 (2020) 118755.
[161] X. Yuan, C. Zheng, Z. Xu, Q. Yang, T. Zhang, X. Luo, H. Zhao, Proc. Combust. Inst. 39 (2022) 5637–5645.
[162] M. Ismael, Y. Wu, M. Wark, New J. Chem. 43 (2019) 4455.
[163] K. Cho, H. Chang, J.H. Park, B.G. Kim, H.D. Jang, J. Ind. Eng. Chem. 14 (2008) 860–863.
[164] L.Q. Jing, X.J. Sun, W.M. Cai, X.Q. Li, H.G. Fu, H.G. Hou, N.Y. Fan, Acta Chim. Sin. 61 (2003) 1241–1245.
[165] C. Chaisuk, A. Wehatoranawee, S. Preampiyawat, S. Netiphat, A. Shotipruk, J. Panpranot, B. Jongsomjit, O. Mekasuwandumrong, Ceram. Int. 37 (2011) 1459–1463.
[166] L. Bertus, C. Faure, A. Danine, C. Labrugère, G. Campet, A. Rougier, A. Duta, Mater. Chem. Phys. 140 (2013) 49–59.
[167] H. Zheng, J.Z. Ou, M.S. Strano, R.B. Kaner, A. Mitchell, K. Kalanta-zadeh, Adv. Funct. Mater. 21 (2011) 2175–2196.
[168] O. Arutanti, A.B.D. Nandiyanto, T. Ogi, F. Iskandar, T.O. Kim, K. Okuyama, J. Alloys Compd. 591 (2014) 121–126.
[169] B. Sun, P.E. Reddy, G.P. Smirniotis, P. G. Sci. Technol. 39 (2005) 6251.
[170] R.N.S. Inturi, M. Suidan, G.P. Smirniotis, Appl. Catal. B Environ. 180 (2016) 351.
[171] C.F. Marques, C.M. Canela, M.A. Stumbo, Catal. Today 133 (2008) 594.
[172] R.V. Elias, G.E. Vaschetto, K. Sapag, E.M. Crivello, G.S. Casuscelli, A.G. Eimer, Top. Catal. 54 (2011) 277.
[173] S.N.R. Inturi, T. Boningari, M. Suidan, P.G. Smirniotis, Ind. Eng. Chem. Res. 55 (46) (2016) 11839–11849.
[174] S.N.R. Inturi, M. Suidan, P.G. Smirniotis, Appl. Catal. B Environ. 180 (2016) 351–361.
[175] S.N.R. Inturi, T. Boningari, M. Suidan, P.G. Smirniotis, J. Phys. Chem. C 118 (2014) 231–242.
[176] H. Zhou, P. Li, J. Liu, Z. Chen, L. Liu, D. Dontsova, R. Yan, T. Fan, D. Zhang, J. Ye, Nano Energy 25 (2016) 128–135.
[177] National Aeronautics and Space Administration (NASA) USA, Climate Change: Vital Signs of the planet: carbon dioxide. http://climate.nasa.gov/vital-signs/carbon-dioxide/, 2016 (accessed 13 September 2016).
[178] T.-M. Su, Z.-Z. Qin, H.-B. Ji, Y.-X. Jiang, G. Huang, Environ. Chem. Lett. 14 (2016) 99–112.
[179] J.G. Yu, J.X. Low, W. Xiao, P. Zhou, J. Am. Chem. Soc. 136 (2014) 8839–8842.
[180] S. Ye, R. Wang, M.-Z. Wu, Y.-P. Yuan, Appl. Surf. Sci. 358 (2015) 15–27.
[181] E.V. Kondratenko, G. Mul, J. Baltrusaitis, G.O. Larrazábal, J. Pérez-Ramírez, Energy Environ. Sci. 6 (2013) 3112–3135.
[182] T. Inoue, A. Fujishima, S. Konishi, K. Honda, Nature. 277 (1979) 637–638.
[183] L.C. Sim, K.H. Leong, P. Saravanan, S. Ibrahim, Appl. Surf. Sci. 358 (2015) 122–129.
[184] S. Ijaz, M.F. Ehsan, M.N. Ashiq, N. Karamat, T. He, Appl. Surf. Sci. 390 (2016) 550–559.
[185] P. Li, H. Jing, J. Xu, C. Wu, H. Peng, J. Lu, F. Lu, Nanoscale. 6 (2014) 11380–11386.
[186] W.-J. Ong, L.K. Putri, L.-L. Tan, S.-P. Chai, S.-T. Yong, Appl. Catal. B Environ. 180 (2016) 530–543.
[187] S. Murcia-López, V. Vaiano, M. Hidalgo, J. Navío, D. Sannino, Photochem. Photobiol. Sci. 14 (2015) 678–685.
[188] F. Li, L. Zhang, J. Tong, Y. Liu, S. Xu, Y. Cao, S. Cao, Nano Energy 27 (2016) 320–329.
[189] B. Yu, Y. Zhou, P. Li, W. Tu, P. Li, L. Tang, J. Ye, Z. Zou, Nanoscale. 8 (2016) 11870–11874.
[190] J. Low, B. Cheng, J. Yu, Appl. Surf. Sci. 392 (2017) 658–686.
[191] J. Ângelo, P. Magalhães, L. Andrade, A. Mendes, Appl. Surf. Sci. 387 (2016) 183–189.
[192] X. Li, H. Liu, D. Luo, J. Li, Y. Huang, H. Li, Y. Fang, Y. Xu, L. Zhu, Chem. Eng. J. 180 (2012) 151–158.
[193] J. Kapica-Kozar, E. Kusiak-Nejman, A. Wanag, Ł. Kowalczyk, R.J. Wrobel, S. Mozia, A.W. Morawski, Microporous Mesoporous Mater. 202 (2015) 241–249.
[194] M. Tahir, N.S. Amin, Energy Convers. Manag. 76 (2013) 194–214.
[195] Y.-P. Yuan, L.-W. Ruan, J. Barber, S.C.J. Loo, C. Xue, Energy Environ. Sci. 7 (2014) 3934–3951.
[196] J.X. Low, J.G. Yu, W.K. Ho, J. Phys. Chem. Lett. 6 (2015) 4244–4251.
[197] X. Li, J.Q. Wen, J.X. Low, Y.P. Fang, J.G. Yu, Sci. China Mater. 57 (2014) 70–100.
[198] A. Cybula, M. Klein, A. Zaleska, Appl. Catal. B Environ. 164 (2015) 433–442.
[199] C. Wang, X. Zhang, Y. Liu, Appl. Surf. Sci. 358 (2015) 28–45.
[200] M. Tahir, N.S. Amin, Appl. Catal. A Gen. 493 (2015) 90–102.
[201] Z. Xiong, Z. Lei, X. Chen, B. Gong, Y. Zhao, J. Zhang, C. Zheng, J.C.S. Wu, Catal. Commun. 96 (2017) 1–5.
[202] D. Kong, J.Z.Y. Tan, F. Yang, J. Zeng, X. Zhang, Appl. Surf. Sci. 277 (2013) 105–110.
[203] L. Liu, F. Gao, H. Zhao, Y. Li, Appl. Catal. B Environ. 134-135 (2013) 349–358.
[204] Q. Zhang, T. Gao, J.M. Andino, Y. Li, Appl. Catal. B Environ. 123–124 (2012) 257–264.
[205] Z. Xiong, Z. Lei, C.-C. Kuang, X. Chen, B. Gong, Y. Zhao, J. Zhang, C. Zheng, J.C. S. Wu, Appl. Catal. B Environ. 202 (2017) 695–703.
[206] Z. Xiong, Z. Xu, Y. Li, L. Dong, J. Wang, J. Zhao, X. Chen, Y. Zhao, H. Zhao, J. Zhang, Appl. Surf. Sci. 507 (2020) 145095.
[207] S.D. Beevers, E. Westmoreland, M.C. de Jong, M.L. Williams, D.C. Carslaw, Atmos. Environ. 54 (2012) 107–116.
[208] K. Fujiwara, S.E. Pratsinis, Appl. Catal. B-Environ. 226 (2018) 127–134.
[209] Y. Zeng, E. Almatrafi, W. Xia, B. Song, W. Xiong, M. Cheng, Z. Wang, Y. Liang, G. Zeng, C. Zhou, Coord. Chem. Rev. 475 (2023) 214874.
[210] C. Zhou, Y. Liang, W. Xia, E. Almatrafi, B. Song, Z. Wang, Y. Zeng, Y. Yang, Y. Shang, C. Wang, G. Zeng, J. Hazard. Mater. 441 (2023) 129871.
[211] X. Li, B. Wang, Y. Cao, S. Zhao, H. Wang, X. Feng, J. Zhou, X. Ma, ACS Sustain. Chem. Eng. 7 (5) (2019) 4548–4563.
[212] M. Ismael, J. Photochem. Photobiol. A Chem. 439 (2023) 114576.
[213] M. Ismael, Inorg. Chem. Commun. 151 (2023) 110607.
[214] C. Zhou, E. Almatrafi, X. Tang, B. Shao, W. Xia, B. Song, W. Xiong, W. Wang, H. Guo, S. Chen, G. Zeng, Sep. Purif. Technol. 286 (2022) 120464.
[215] J. Tollefson, Nature. 551 (2017) 283.
[216] S. Ali, J. Lee, H. Kim, Y. Hwang, A. Razzaq, J.W. Jung, C.H. Cho, S. Il In, Appl. Catal. B Environ. 279 (2020) 119344.
[217] Y. Li, J. Hao, H. Song, F. Zhang, X. Bai, X. Meng, H. Zhang, S. Wang, Y. Hu, J. Ye, Nat. Commun. 10 (2019) 1–9.
[218] Y. Yang, J. Liu, F. Liu, Fuel. 276 (2020) 118093.
[219] S.O. Kobald, E. Wascher, M. Blaszkewicz, K. Golka, C. van Thriel, Neurobehav. Toxicol. 48 (2015) 50–59.
[220] L. Meng, H. Zhao, Appl. Catal. B Environ. 264 (2020) 118427.
[221] G. Merle, M. Wessling, K. Nijmeijer, J. Membr. Sci. 377 (2011) 1–35.
[222] X.X. Zou, Y. Zhang, Chem. Soc. Rev. 44 (2015) 5148–5180.
[223] X. Zhao, Y. Hu, H. Jiang, J. Yu, R. Jiang, C. Li, Nanoscale 10 (2018) 13384–13392.
[224] N. Wang, F. Niu, S. Wang, Y. Huang, Particuology. 41 (2018) 58–64.
[225] B. Pongthawornsakun, O. Mekasuwandumrong, F.J.C. Santos Aires, R. Büchel, A. Baiker, S.E. Pratsinis, J. Panpranot, Appl. Catal. A-Gen. 549 (2018) 1–7.
[226] E. Bahadori, A. Tripodi, G. Ramis, I. Rossetti, ChemCatChem. 11 (2019) 4642–4652.
[227] P.G. Smirniotis, T. Boningari, D. Damma, S.N.R. Inturi, Catal. Commun. 113 (2018) 1–5.
[228] B.-J. Kim, E. Fabbri, I. Castelli, M. Borlaf, T. Graule, M. Nachtegaal, T. Schmidt, Catalysts. 9 (2019) 263.
[229] Y.-J. Wang, C. Liu, Y.-J. Wu, Y.-H. Song, M.-L. Zhu, J. Huang, Z.-T. Liu, Z.-W. Liu, Catal. Today 339 (2020) 40–47.
[230] J. Horlyck, S. Lewis, R. Amal, J. Scott, Top. Catal. 61 (2018) 1842–1855.
[231] S. Tada, K. Fujiwara, T. Yamamura, M. Nishijima, S. Uchida, R. Kikuchi, Chem. Eng. J. 381 (2020) 122750.
[232] G.K. Beh, C.T. Wang, K. Kim, J. Qu, J. Cairney, Y.H. Ng, A.K. An, R. Ryoo, A. Urakawa, W.Y. Teoh, Green Chem. 22 (2020) 688–698.
[233] M. Macino, A.J. Barnes, S.M. Althahban, R. Qu, E.K. Gibson, D.J. Morgan, S. J. Freakley, N. Dimitratos, C.J. Kiely, X. Gao, A.M. Beale, D. Bethell, Q. He, M. Sankar, G.J. Hutchings, Nat. Catal. 2 (2019) 873–881.
[234] H.-U. Blaser, H. Steiner, M. Studer, Chem. Catal. Chem. 1 (2009) 210–221.
[235] R.M. Deshpande, A.N. Mahajan, M.M. Diwakar, P.S. Ozarde, R.V. Chaudhari, J. Organomet. Chem. 69 (2004) 4835–4838.
[236] Y. Xu, Y. Liu, P. Cui, N. Shang, C. Wang, Y. Gao, J. Appl. Catal. A: Gen. 622 (2021) 118230.
[237] M.J. Beier, J.-M. Andanson, A. Baiker, ACS Catal. 2 (2012) 2587–2595.
[238] S. Pisduangdaw, J. Panpranot, C. Methastidsook, C. Chaisuk, K. Faungnawakij, P. Praserthdam, O. Mekasuwandumrong, Appl. Catal. A Gen. 370 (2009) 1–6.
[239] S. Somboonthanakij, O. Mekasuwandumrong, J. Panpranot, T. Nimmanwudtipong, R. Strobel, S. Pratsinis, P. Praserthdam, Catal. Lett. 119 (2007) 346–352.
[240] A. Corma, P. Serna, P. Concepción, J.J. Calvino, J. Am. Chem. Soc. 130 (2008) 8748–8753.
[241] S. Bhogeswararao, D. Srinivas, J. Catal. 285 (2012) 31–40.
[242] N.M. Bertero, A.F. Trasarti, B. Moraweck, A. Borgna, A.J. Marchi, Appl. Catal. A Gen. 358 (2009) 32–41.
[243] S. Pisduangdaw, O. Mekasuwandumrong, S.I. Fujita, M. Arai, H. Yoshida, J. Panpranot, Catal. Commun. 61 (2015) 11–15.
[244] S. Pisduangdaw, O. Mekasuwandumrong, H. Yoshida, S.I. Fujita, M. Arai, J. Panpranot, Appl. Catal. A Gen. 490 (2015) 193–200.
[245] M. Al-Herz, M.J.H. Simmons, J. Wood, Ind. Eng. Chem. Res. 51 (2012) 8815–8825.

[246] N.P. Rylander, Hydrogenation Methods, Academic Press, New York, 1985.
[247] J. Panpranot, K. Phandinthong, T. Sirikajorn, M. Arai, P. Praserthdam, J. Mol. Catal. 261 (2007) 29.
[248] J.A. Bennett, N.J. Creamer, K. Deplanche, L.E. Macaskie, I.J. Shannon, J. Wood, Chem. Eng. J. 65 (2010) 282–290.
[249] S. Dominguez-Dominguez, A. Berenguer-Murcia, D. Cazorla-Amoros, A. Linares-Solano, J. Catal. 243 (2006) 74.
[250] P. Weerachawanasak, O. Mekasuwandumrong, M. Arai, I.S. Fujita, P. Praserthdam, J. Panpranot, J. Catal. 262 (2009) 199.
[251] J.A. Lopez-Sanchez, N. Dimitratos, N. Glanville, L. Kesavan, C. Hammond, J. K. Edwards, A.F. Carley, C.J. Kiely, G.J. Hutchings, Appl. Catal. A Gen. 391 (2011) 400–406.
[252] M. Conte, A.F. Carley, G. Attard, A.A. Herzing, C.J. Kiely, G.J. Hutchings, J. Catal. 257 (2008) 190–198.
[253] A.M. Venezia, V. La Parola, G. Deganello, B. Pawelec, J.L.G. Fierro, J. Catal. 215 (2003) 317–325.
[254] P.G.N. Mertens, S.L.F. Corthals, X. Ye, H. Poelman, P.A. Jacobs, B.F. Sels, I.F. J. Vankelecom, D.E. De Vos, J. Mol. Catal. A Chem. 313 (2009) 14–21.
[255] S. Bawaked, Q. He, N.F. Dummer, A.F. Carley, D.W. Knight, D. Bethell, C.J. Kiely, G.J. Hutchings, Catal. Sci. Technol. 1 (2011) 747–759.
[256] N.F. Dummer, S. Bawaked, J. Hayward, R. Jenkins, G.J. Hutchings, Catal. Today 154 (2010) 2–6.
[257] X. Yang, D. Chen, S. Liao, H. Song, Y. Li, Z. Fu, Y. Su, J. Catal. 291 (2012) 36–43.
[258] P.J. Miedziak, Q. He, J.K. Edwards, S.H. Taylor, D.W. Knight, B. Tarbit, C.J. Kiely, G.J. Hutchings, Catal. Today 163 (2011) 47–54.
[259] B. Pongthawornsakun, S.I. Fujita, M. Arai, O. Mekasuwandumrong, J. Panpranot, Appl. Catal. A Gen. 467 (2013) 132–141.
[260] B. Pongthawornsakun, O. Mekasuwandumrong, S. Prakash, E. Ehret, F.J.C. S. Aires, J. Panpranot, Appl. Catal. A Gen. 506 (2015) 278–287.
[261] K. Fulajtárova, T. Soták, M. Hronec, I. Vávra, E. Dobrocka, M. Omastová, Appl. Catal. A Gen. 502 (2015) 78–85.
[262] M. Besson, P. Gallezot, C. Pinel, Chem. Rev. 114 (2014) 1827–1870.
[263] M.M. Villaverde, N.M. Bertero, A.J. Marchi, T.F. Garetto, Catal. Today 213 (2013) 87–92.
[264] B.M. Nagaraja, et al., Catal. Commun. 4 (6) (2003) 287–293.
[265] J.J. Musci, B.A. Merlo, L.M. Casella, Catal. Today 296 (2017) 43–50.
[266] Y. Wang, Y. Miao, S. Li, L. Gao, G. Xiao, Mol. Catal. 436 (2017) 128–137.
[267] M.R. Mironenko, et al., Catal. Today 249 (2015) 145–152.
[268] L. Liu, H. Lou, M. Chen, Appl. Catal. A Gen. 550 (2018) 1–10.
[269] W. Tolek, K. Khruechao, B. Pongthawornsakun, O. Mekasuwandumrong, F.J.C. S. Aires, P. Weerachawanasak, J. Panpranot, Catal. Commun. 149 (2021) 106246.
[270] B. Nematollahi, M. Rezaei, E.N. Lay, J. Rare Earths 33 (2015) 619–628.
[271] S. Dey, G.C. Dhal, D. Mohan, R. Prasad, Chem. Reaction Eng. Catal. 12 (3) (2017) 370–383.
[272] D. Chen, Z. Qu, Y. Sun, K. Gao, Y. Wang, Appl. Catal. B Environ. 142–143 (2013) 838–848.
[273] P. Schlexer, D. Widmann, R. Jürgen, G. Pacchioni, ACS Catal. 8 (7) (2018) 6513–6525.
[274] S.M. McClure, D.W. Goodman, Chem. Phys. Lett. 469 (2009) 1–13.
[275] P. Kast, M. Friedrich, F. Girgsdies, J. Kröhnert, D. Teschner, T. Lunkenbein, M. Behrens, R. Schlögl, Catal. Today 206 (2016) 21–31.
[276] G. Tofighi, X. Yu, H. Lichtenberg, D.E. Doronkin, W. Wang, C. Woell, Y. Wang, J. D. Grunwaldt, ACS Catal. 9 (2019) 5462–5473.
[277] K. Dadir, S.H. Kim, S.M. Kim, H. Ha, J.Y. Park, J. Phys. Chem. C 116 (2012) 24054–24059.
[278] L. Liu, F. Zhou, L. Wang, X. Qi, F. Shi, Y. Deng, J. Catal. 274 (2010) 1–10.
[279] J. Kim, Y. Kim, M.H. Wiebenga, S.H. Oh, D.H. Kim, Appl. Catal. B Environ. 251 (2019) 283–294.
[280] R. Kydd, W.Y. Teoh, K. Wong, Y. Wang, J. Scott, Q.-H. Zeng, A.-B. Yu, J. Zou, R. Amal, Adv. Funct. Mater. 19 (2009) 369–377.
[281] J. Zhang, H. Li, J. Ye, Z. Cao, J. Chen, Q. Kuang, J. Zheng, Z. Xie, Nano Energy 61 (2019) 397–403.
[282] R.P. Doherty, J.-M. Krafft, C. Methivier, S. Casale, H. Remita, C. Louis, C. Thomas, J. Catal. 287 (2012) 102–113.
[283] F. Muench, G.A. El-Nagar, T. Tichter, A. Zintler, U. Kunz, L. Molina-Luna, V. Sikolenko, C. Pasquini, I. Lauermann, C. Roth, ACS Appl. Mater. Interfaces 11 (2019) 43081–43092.
[284] S. Hannemann, J.-D. Grunwaldt, P. Lienemann, D. Guenther, F. Krumeich, S. E. Pratsinis, A. Baiker, Appl. Catal. A Gen. 316 (2007) 226–239.
[285] J. Jiang, J. Lei, Y. Hua, W. Bi, N. Xu, Y. Lia, X. Chen, H. Jiang, C. Li, Appl. Surf. Sci. 521 (2020) 146447.
[286] W. Bi, Y. Hu, H. Jiang, H. Yu, W. Li, C. Li, Appl. Surf. Sci. 481 (2019) 360–368.
[287] B. Kucharczyk, W. Tylus, J. Okal, J. Checmanowski, B. Szczygieł, Chem. Eng. J. 309 (2016) 288–297.
[288] S. Royer, D. Duprez, ChemCatChem. 3 (2011) 24–65.
[289] C. Galeano, R. Güttel, M. Paul, P. Arnal, A.H. Lu, F. Schüth, Chem. Eur. J. 17 (2011) 8434–8439.
[290] D. Widmann, R.J. Behm, Acc. Chem. Res. 74 (2014) 740–749.
[291] M.Y. Kang, H.J. Yun, S. Yu, W. Kim, N.D. Kim, J. Yi, J. Mol. Catal. A Chem. 368-369 (2013) 72–77.
[292] X. Chen, Z. Xu, F. Yang, H. Zhao, Proc. Combust. Inst. 37 (2019) 5499–5506.
[293] A. Elmhamdi, R. Castañeda, A. Kubacka, L. Pascual, K. Nahdi, A. Martínez-Arias, Appl. Catal. B: Environ. 188 (2016) 292–304.
[294] D. Wang, D. Astruc, Chem. Soc. Rev. 46 (3) (2017) 816–854.
[295] X. Yuan, M. Qing, L. Meng, H. Zhao, Energy Fuel 24 (2020) 14447–14457.
[296] A. Sukee, A.A. Alharbi, A. Staerz, A. Wisitsoraat, C. Liewhiran, U. Weimar, N. Barsan, Actuator B-Chem. 312 (2020).
[297] S.H. Choi, Y.C. Kang, Nanoscale 5 (2013) 4662–4668.
[298] G.Y. Liu, S.K. Karuturi, H.J. Chen, L. Spiccia, H.H. Tan, C. Jagadish, D.W. Wang, A.N. Simonov, A. Tricoli, Nano Energy 53 (2018) 745–752.
[299] G.A. Sotiriou, D. Franco, D. Poulikakos, A. Ferrari, ACS Nano 6 (2012) 3888–3897.